Experimental Low Cost Reflective Type Oximeter for Wearable Health Systems

Eduardo M. G. Rodrigues [a], Radu Godina [a], Carlos M. P. Cabrita [b], João P. S. Catalão [a,c,d*]

[a] C-MAST, University of Beira Interior, R. Fonte do Lameiro, 6201-001 Covilhã, Portugal
[b] CISE, University of Beira Interior, R. Fonte do Lameiro, 6201-001 Covilhã, Portugal
[c] INESC TEC and Faculty of Engineering of the University of Porto, R. Dr. Roberto Frias, 4200-465 Porto, Portugal
[d] INESC-ID, Instituto Superior Técnico, University of Lisbon, Av. Rovisco Pais, 1, 1049-001 Lisbon, Portugal

Abstract

The advent of wearable technology is fundamental to the dissemination of wearable personal health monitoring devices. Recent developments of biomedical sensors have decreased the form factor and power consumption that can be worn on a permanent basis. This paper discusses a low cost reflective photoplethysmography (PPG) system using a dedicated integrated circuit (IC) solution as the core of a wearable health monitoring device. The measurement of two physiological indicators is performed, namely the pulse rate (HR) and the blood oxygen saturation (SpO_2). The paper analyses in depth the PPG signals sensing architecture, guaranteeing high resolution measurements due to a delta-sigma analog to digital conversion unit. Post-processing digital filter operations are implemented to enhance low noise PPGs acquisition for physiological signals extraction. A complete system design is presented and a detailed evaluation is made in a real-time processing scenario. The test platform is completed with a PC based graphics application for on-line and off-line data analysis. Minimizing power dissipation is the main challenge in a wearable design. However, it restrains PPG signal measurement sensitivity by lowering signal quality. Using the developed prototype power consumption, studies concerning the characterization of power consumption and signal quality over various working conditions are performed. Next, a performance merit figure is proposed as the main research contribution, which addresses the power consumption and signal quality trade-off subject. It aims to be used as an analysis for trade-offs between these two conflicting design criteria.

Keywords: Wearable health systems; Reflective pulse oximeter; Biomedical sensor; Digital signal processing; Signal acquisition; Signal quality.

1. Introduction

Sensors for health monitoring have been used for decades in the conventional healthcare network. Whether being utilised for the diagnosis and prevention of the patient or being employed in cases where the patient is bedridden, these signal sensing tools play a crucial role in modern healthcare services. Until few years ago these sensing tools were exclusively part of the hospitals and major private clinics. Despite being portable to a certain extent they had a specific function of monitoring a bedridden patient or with limited mobility. From the functionality point of view, they were used and are still being used as static sensing devices.

With increasing reduction of the size of silicon manufactured electronics chips, the design of dedicated ICs for health monitoring is now feasible as more and more functions are integrated in a tiny silicon area providing advanced functionality at low cost [1].

Pulse oximetry is a non-invasive method that compares how much red (RED) and infrared (IR) light are absorbed by blood vessels and serves as the basis for measuring SpO_2 [2] [3]. In addition, the detected IR signal variable component related to arterial part can be used to determine the subject HR [4]. Portable pulse oximeter systems are currently utilised in hospitals, which can be transported around by the patient under investigation. The measurements are typically made at the extremities of the body. Consequently, the sensor is applied to peripheral parts of the human body [5].

Several studies were performed in the literature regarding such type of devices. In [6] developed algorithms for automated quality assessment for pulse oximetry and blood pressure signals were tested retrospectively with data acquired from a trial that recorded signals in a home environment. The development of an Electronic Patch - a new health monitoring system incorporating biomedical sensors, microelectronics, radio frequency communication, and a battery embedded in a 3-dimensional hydrocolloid polymer is reported in [7] for wearable health monitoring. In [8] is presented through a prototype a power optimised PPG sensor interface to sense arterial oxygen saturation, a technique to dynamically trade off signal-to-noise ratio (SNR) for power during sensor operation, and a simple

* Corresponding author at: Faculty of Engineering of the University of Porto, R. Dr. Roberto Frias, 4200-465 Porto, Portugal. *Email address:* catalao@ubi.pt (João P.S. Catalão).

algorithm to choose when to acquire samples in PPG. In [9] a ring-shaped photodiode designed for use in a reflectance pulse oximetry sensor in wireless health monitoring applications is presented. A study which investigates the effects of local tissue and room temperature conditions on PPG signal quality as applied to pulse oximeters using transmittance sensors for 20 healthy adult volunteers is proposed in [5]. In [10] is presented a novel cross-coupled sigma delta modulator which ensures that measurement accuracy will be more robust in comparison with conventional fixed-frequency oximeter modulation technique especially in the presence of pulsed artificial ambient light. Moreover, this novel modulator gives an extra control over the pulse oximeter power consumption leading to improved power management. In [2] is given the results from a study showing the ability of the Gaussian basis representation to extract heart rate and respiratory rate from PPG signal where several simulation experiments have been used to demonstrate that the Gaussian decomposition results in a highly efficient method for the representation of PPG signals. An ultra-low-power pulse oximeter suited for portable medical applications implemented with an energy-efficient transimpedance amplifier is proposed in [11]. In [3] is presented a small, low-cost pulse oximeter design appropriate for wearable and surface-based applications that also produces quality, unfiltered PPGs ideal for emerging diagnostic algorithms while being distinct from conventional pulse oximeters that incorporate filters for signal extraction and noise reduction. In [12] is developed a unique on-board feature detection algorithm to assess the quality of PPGs acquired with a custom reflectance mode, wireless pulse oximeter. In [13] is proposed the implementation of the first fully integrated pulse oximeter front-end with power consumption lower than 1 mW enabled by system- and block-level noise optimisation. In [14] is designed a wearable pulse oximeter a novel algorithm is proposed where a minimum correlation discrete saturation transform has been developed for the estimation of arterial oxygen saturation, based on an optical model derived from photon diffusion analysis. In [15] is presented a new method that uses the pulse oximeter signal to estimate the respiratory rate and the method uses a recently developed time-frequency spectral estimation method, variable-frequency complex demodulation to identify frequency modulation (FM) of the PPG waveform. A novel approach using time–frequency analysis of pulse-oximeter data to detect progressive hypovolemia in spontaneously breathing healthy subjects is proposed in [16]. In [17] is presented a particle filtering algorithm for respiratory rate extraction from pulse oximeter, which combines both time-invariant and time-varying autoregressive models for accurate extraction of breathing frequencies that vary either slowly or suddenly. In [18] is proposed a novel method for estimating respiratory rate in real time from the PPG obtained from pulse oximetry where three respiratory-induced variations (frequency, intensity, and amplitude) are extracted from the PPG using the Incremental-Merge Segmentation algorithm. Finally, a novel approach for motion artefact reduction in PPG signals based on AS-LMS adaptive filter is presented in [19].

An increasingly number of handheld pulse oximeters currently exist for fitness segment and health domestic applications. The common type use is the transmittance of light through a finger [20]. The wrist-finger model is noticeably ordinary in the market as well. The appliance is in fact a finger model since the sensor is positioned on a finger which is consequently attached to a wrist display. However, the pulse oximeter on the finger is relatively visible and the finger might not be entirely comfortable for extended periods and nonstop monitoring [21]. There are some disadvantages such as the recurrent addition of movement artefacts intercede particularly with long term monitoring of a subject [22]. Another shortcoming is the low quality of the signal in the incident of centralisation in cases in which the subject suffers from sepsis, coldness, shock or cardio-pulmonary anomalies [23]. On the other hand, such occurrences are the highest application scenarios of portable SpO_2 monitors [24]. Reflectance principle operated pulse oximetry is other form of implementation. The reflection one appears to be more capable since is possible to measure any area on the skin surface [25]. Conversely, in the case of oximeters of reflection nature, the reasonably great background (BG) light incident on the light detector and the poor reflection signal acquired from the skin surface exclude precise measurements [26]. Nevertheless, wearable devices by reflectance pulse oximetry will gain more and more acceptance from the domestic market. Several semiconductor manufacturers are targeting this market by releasing sophisticated dedicated units for such purposes. The great level of miniaturisation signifies that a robust and reliable oximeter comprising a microcontroller unit (MCU), biomedical sensors and advanced wireless communication characteristics can be combined into a very small physical device [27].

In this paper a low-power reflective pulse oximeter prototype is presented and built with a dedicated analog front end (AFE) circuitry with post-processing digital techniques based signal extraction performed by a low power high performance MCU. Real time software routines ensure continuous processing of HR and SpO_2 and raw PPG data are delivered to a workstation. Full wearable pulse oximetry requires ultra-low power dissipation since energy is provided by a small size battery. To keep low the average power consumption high strength of the signal received at the photodetector circuit cannot be guaranteed since SNR is negatively affected with short LEDs on-time [28]. In this regard, two research lines were developed in this paper. First, the oximeter design is scrutinised in two areas: signal quality measurement considering LEDs current values full scale and power consumption characterization in the same LEDs current range. Since the SoC's analog digital converter (ADC) can be operated

with different resolutions its impact on oximeter performance is measured for the same evaluation parameters mentioned above. For this purpose the highest and lowest ADC resolutions were chosen. Secondly, a novel technique aimed to perform power consumption to signal quality trade-off is described. On the basis of the information collected above, a ratio is created and mapped for the LEDs current full range. It quantifies how much power is required to code the PPG AC term per digitization level (bit).

The paper is organised as follows. The challenges regarding a fully wearable oximeter design are identified and discussed in Section II. The pulse oximetry theory is described in Section III. Section IV details system design. Section V contains the tests performed on the prototype board and provides results discussion. Finally, the conclusions are summarised in Section V.

2. Challenges on Wearable Oximeter Design

A fully wearable photoplethysmographic HR and SpO_2 monitoring equipment can be challenging since several constraints should be fulfilled such as small design size, easy to incorporate in clothes or externally attached to the body, its use pass unnoticed from user view point and requiring a battery change after a long period of continuous use. High-end performance oximeter for professional usage presents high resilience to ambient light and or motion artefacts and excellent accuracy [29]. All this come at a price – energy consumption requirement is not necessary a priority target. However, for a wearable sensing device lowering the oximeter power consumption is critical. Several strategies are proposed in literature for handling energy consumption issue [13].

At core of an oximetry sensor the front-end design consists of a single photodiode at the detector end, a transimpedance amplifier (TIA) as photoreceptor and a signal conditioning stage to filter the noise outside the frequency band of interest and to match the PPG signal amplitude to the ADC input range. Furthermore, a LEDs driver circuit is part of the design, generating two modulated light output. The signal processing algorithms to estimate the quantities of interest, which are SpO_2 and HR are carried out by MCU. The PPG signal quality depends on the resolution employed to measure the photocurrent. In other words, the level of sensitivity regarding the oximeter analog front-end is typically described in terms of SNR. Therefore, PPG readings with adequate SNR imply low noise analog front-end design [30]. Oximetry devices have different noise sources that contribute to limit the SNR performance. Consequently, if the objective is to maximize the SNR at low duty cycle then becomes necessary to carefully design the signal path. Thus, in order to design low cost wearable oximeters a trade-off between power and accuracy has to be made. With this approach, LEDs current regulation is the main contributor for power consumption. At the other side of the spectrum, noise sources are related to the normal noise of the photodiode, the voltage source used to reverse-bias the photodiode, TIA feedback resistors thermal noise, the switched-integrator along the voltage-mode operational amplifier [13]. Fig. 1 highlights the pros and cons of the trade-off that has to be made given the initial goals when designing the oximeter.

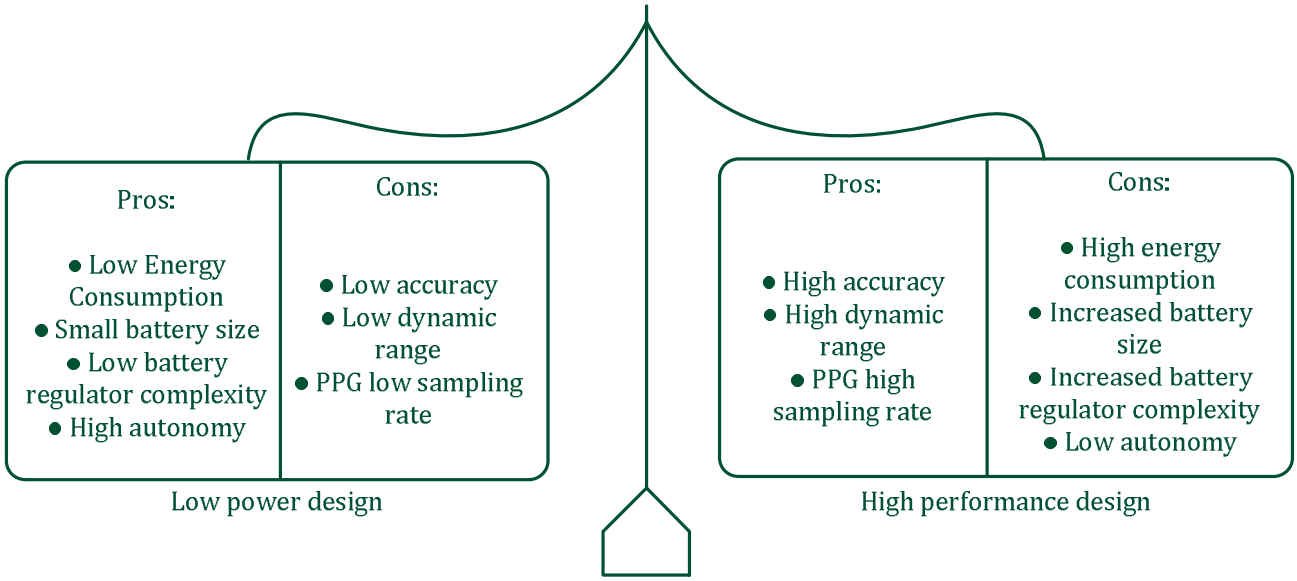

Fig. 1. Pros and cons of the trade-off between two design views.

Conventional portable oximetry systems are typically built using excitation LED units, a photodetector interface circuit and a precision ADC module operated by a MCU that extract the AC and DC components of the plethysmography signals. Despite the small size of the components discrete circuitry a considerable print circuit board area is required. In order to address today trends toward smaller electronics devices without compromising the performance, efforts have been made to integrate as much as possible the various elements of the dedicated circuitry in miniature form into a single silicon unit. This kind of high integration and specialised circuitry is popularly known as System on Chip (SoC).

For wearable health applications the oximetry technology should present very small form factor without causing discomfort with its use. Furthermore, to be portable its weight should be minimised and its energy consumption profile very restricted which can be considered challenging due to the LED sources [8]. Reflected PPG signals measurement devices as an alternative to transmission pulse oximetry may achieve these qualifications while offering a singular advantage that enable them to be located in different body areas [6]. Several semiconductor manufacturers are targeting this market releasing sophisticated SoC units for this purpose. The high miniaturisation level means that a very capable wearable monitoring system comprising a MCU, biomedical sensors and advanced wireless communication features can be merged into a very small physical device. One important feature of the integrated pulse oximetry is evident by requiring less internal MCU resources since PPGs acquisition and basic signal processing is handled by the SoC. In this sense, the MCU peripheral system can be downsized saving silicon area, thus contributing to a high compact body sensor solution. The level of miniaturisation is illustrated in Fig. 2 where a high compact SoC and at the same time very tiny can perform most of the signal processing functions found on a conventional oximeter. The shown SoC unit is aimed to be used as reflective optical sensor in wearable oximetry [31].

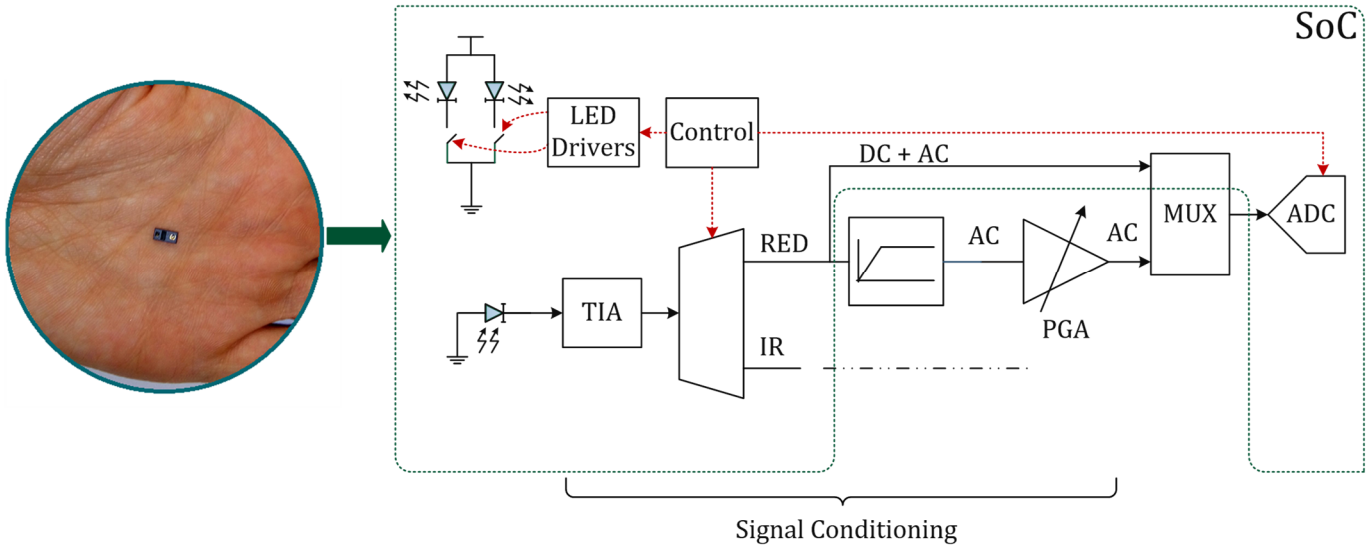

Fig. 2. Typical reflectance pulse oximeter signal conditioning block diagram and functions implemented on a dedicated oximeter SoC.

One important feature of the integrated pulse oximetry is evident by requiring less internal MCU resources since PPGs acquisition and basic signal processing is handled by the SoC. In this sense, the MCU peripheral system can be downsized saving silicon area, thus contributing to a high compact biomedical sensor solution.

3. Pulse Oximetry Principles

When the oxygen (O_2) is in the blood it can be transported in two ways. It can be dissolved in the plasma, which corresponds to 2% of the total value, the reason being that the blood is made essentially by water and that the gases hardly dissolve in such environments. A second and more efficient way is the connection of O_2 to the haemoglobin (Hb) [32].

The saturation of oxyhemoglobin HbO_2 or the functional saturation of O_2 is calculated as follows:

$$SO_2(\%) = \frac{[HbO_2]}{[HbO_2]+[Hb]} \times 100\% \quad (1)$$

Generally, reflectance pulse oximetry operates with two different wavelengths through a tissue with the purpose of measuring the transmitted light signal [33]. Thus, its operation is based on physical principles concerning

behaviour of the light. The values in which the absorption of HbO_2 and Hb present the highest difference of absorption are chosen [8]. Another method is the flattening of the absorption spectrum that aims to minimise the errors associated with the modification of wavelength peaks of the sensor LEDs [34]. The red (RED) band (660nm) and infrared (IR) (880-940nm) are the wavelengths usually used for pulse oximetry. Such wavelengths are selected due to the reason of maximising absorption and limit the margin of error of the device [35].

LEDs can emit wavelength of different intensities, thus, a standardisation of such intensities has to be made. Since the signal DC bias is common for different wavelengths it is possible to obtain a ratio (*R*) between the emitted light of the R and IR LEDs [30]. The HbO_2 saturation is estimated by the following equation which is a ratio of ratios and described by R [11]:

$$R = \frac{\left(\frac{I_{AC}}{I_{DC}}\right)_R}{\left(\frac{I_{AC}}{I_{DC}}\right)_{IR}} \tag{2}$$

where I_{AC} is the time-varying or AC component and I_{DC} is the average term of the received photocurrent of the red and infrared light signals.

By combining equation (2) with the following equations known as the Lambert-Beer law:

$$I_t = I_0 \times e^{-A} \tag{3}$$

$$A = \varepsilon \times D \times c \tag{4}$$

where I_t is the intensity of light that trespasses the medium, I_0 represents the intensity of incident light, A is the absorbance, D represents the distance covered beam of light, ε is the extinction coefficient of the solute (*Hb*) and c represents the concentration of the solute.

Then the equation (5) of S_pO_2 is obtained:

$$\begin{aligned} S_pO_2 = &\left\{-\varepsilon_R(Hb) + \varepsilon_{IR}(Hb) \times \left(\frac{R}{IR}\right)\right\} \times \\ &\left\{\left[\varepsilon_R(HbO_2) - \varepsilon_R(Hb)\right] + \left[\varepsilon_{IR}(Hb) - \varepsilon_{IR}(HbO_2)\right] \times \left(\frac{R}{IR}\right)\right\}^{-1} \end{aligned} \tag{5}$$

where $\varepsilon_R(Hb)$ and $\varepsilon_{IR}(Hb)$ are the extinction coefficients of haemoglobin referred to the RED light. Finally, $\varepsilon_R(HbO_2)$ and $\varepsilon_{RED}(HbO_2)$ are the extinction coefficients of oxyhemoglobin with relation to the RED light.

Even though the Lambert-Beer law is a great basis for pulse oximetry, there are some unforeseen occasions when the measurement of S_pO_2 doesn't follow the law [35].

Since part of the transmitted light is reflected by the blood cells different methods of calibration of oximeters are utilized today. For the calibration of the oximeters the manufacturers resort to data of the S_pO_2 based on studies with volunteers and measured by a medical device through an invasive manner [36]. Many studies were made with the aim to minimise the errors associated to such type of measurement resulting in a modification of the S_pO_2 equation. The relation between *R* and the measured values by the oximeter are made by [8]:

$$SpO_2 = \frac{K_1 - K_2 R}{K_3 - K_4 R} \tag{6}$$

The K_1, K_2, K_3 and K_4 coefficients are obtained experimentally, through in vitro measurements for the best approximation possible [35].

4. System Design

A. General architecture

The system developed in this study comprises a SoC unit, a battery charger and a MCU based board. The prototype design is also set to be connected to other devices through a 2.4GHz wireless infrastructure. A general overview can be observed in Fig. 3.

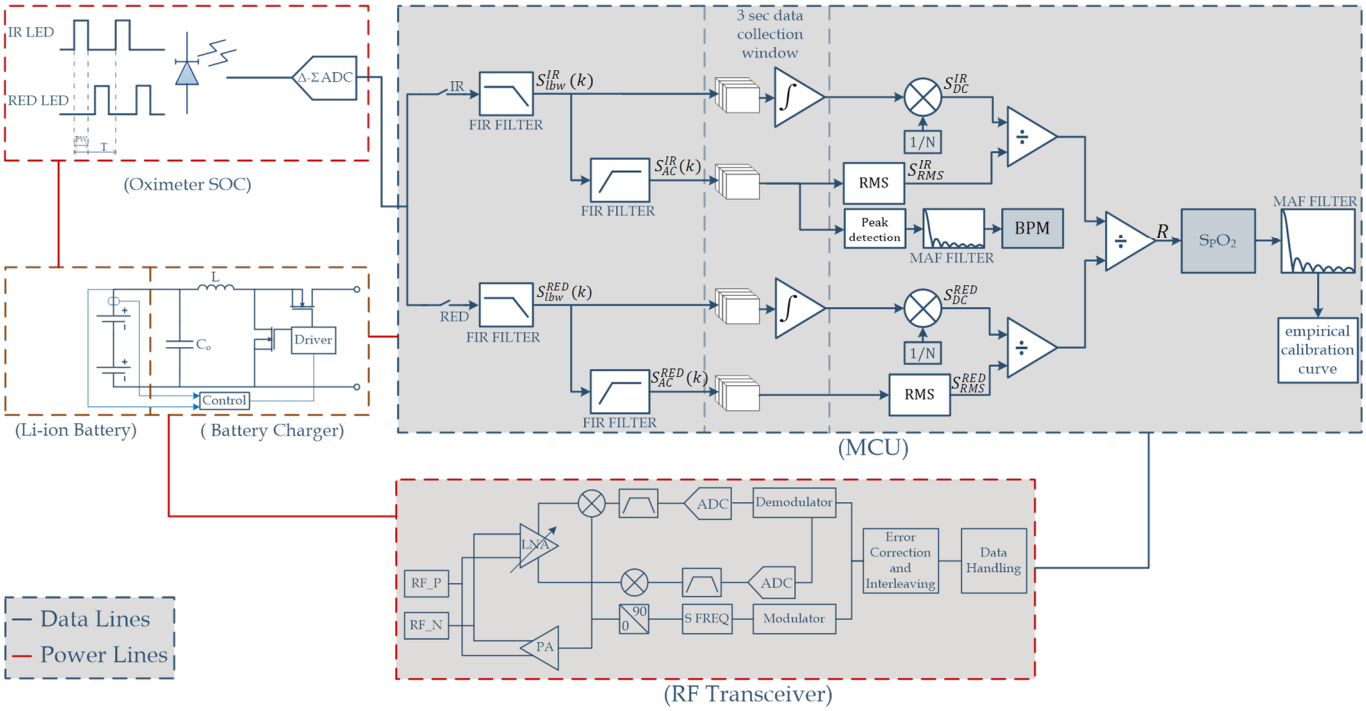

Fig. 3. Global view of oximeter's functional modules.

B. The SoC device

The reflectance pulse oximeter design in this study relies on a MAX30100 SoC unit manufactured by Maxim Integrated [37]. This unit offers two LEDs, photodetector, low-noise analog signal processing functions to minimise ambient light impact and a 16-bit sigma delta ADC. PPGs sampling rate varies between 50sps and 1000sps. ADC dynamic range depends on the LEDs current pulse width. The highest pulse width enables 16-bit digital conversion. Setting the minimum pulse width conversion output does not surpass the 13-bit of resolution.

C. MCU core based signal processing algorithms

Significant signal extraction and noise reduction techniques are already taken by the oximeter SoC. However, there is room for improving the quality of readings if the goal is to maximise high-fidelity PPGs with the existing hardware resources. The block diagram in Fig. 2 highlights the post-processing operations performed by the MCU.

The signal processing main tasks consist of white noise filtering, DC component measurement and AC term extraction of the PPGs. In Fig. 3 the upper digital signal processing chain refers to the signal treatment carried out with IR signals acquired through the SoC's ADC module. The same set of operations is implemented in the lower signal chain, with the exception of the HR measurement block which is performed solely on the IR PPGs AC components.

The maximum dynamic range provided by the oximeter's SoC is 16-bit for 50sps, which is the lowest sampling rate available. The low acquisition rate simplifies any intensive math-intensive applications to be run within a MCU. In order to analyse the post-processing requirements important information can be extracted if the discrete Fourier transform (DFT) algorithm is applied to the PPG raw data. The equation for an N-point DFT is as follows:

$$X(m) = \sum_{n=0}^{N-1} x(n) e^{-j2\pi mn/N} \quad M = 0, \ldots N-1 \tag{7}$$

where $x(n)$ is the sequence of raw PPG samples, N is the number of samples used for computing the DFT output, n is the index of the time-domain index of the incoming samples and m the DTF output index in the frequency domain. A time-series of approximately 26s was collected and analysed via DFT. The DFT bin resolution is

provided by 1310 samples. By taking the magnitude squared of each $X(m)$ term, the power spectrum of both PPG values is shown in Fig. 4.

According to Fig. 4 the spectral content appears close to 10 Hz. As expected, the arterial pulsating part is considerable low in comparison to absorption component due to remaining tissue. For SpO_2 evaluation usable bandwidth starts at 0 Hz and is superiorly limited by the maximum heart rate measurement requirement. Normally, professional heart rate monitoring devices are designed to read up to 300 bpm. Thus practical bandwidth of interest goes as maximum as 5 Hz. Thus, additional frequency removal efforts can be made by applying low pass digital filtering and thus removing unnecessary frequency. For the design in discussion the low pass filter cut-off frequency is set at 3 Hz and stopband starts at 6 Hz. This implies that heart rate tracking is functional up to 180 bpm. Filter stop band level is set at -105 dB. The results can be observed in Fig. 5.

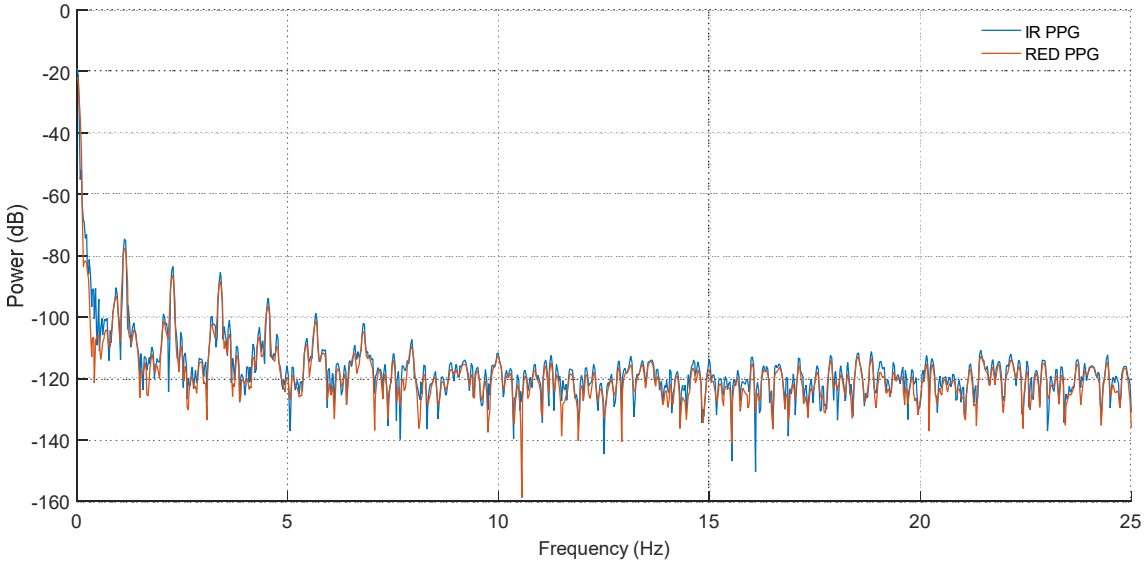

Fig. 4. Power spectrum of acquired PPG signals sampled at f_s = 50 sps.

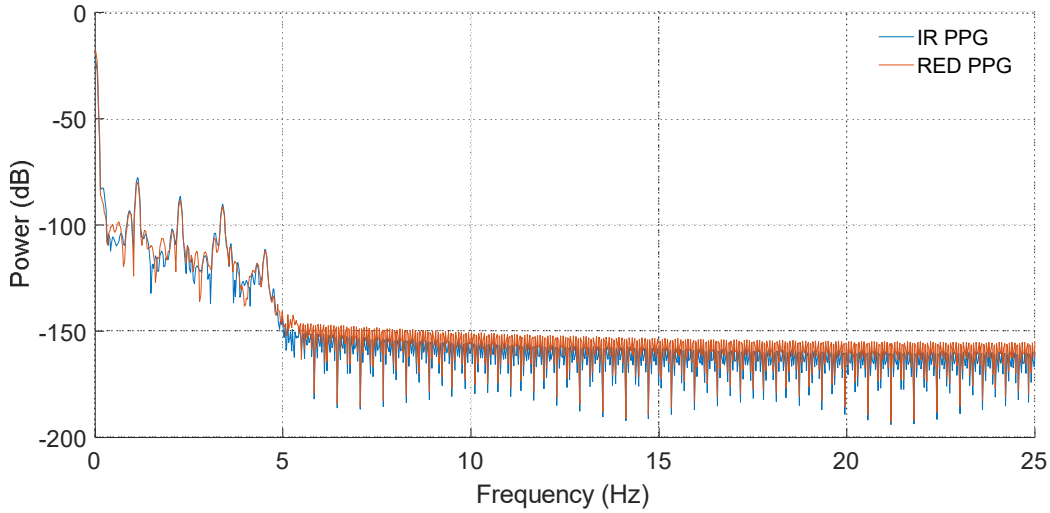

Fig. 5. PPG signals power spectrum after applying a low pass digital filter.

Above 3 Hz the remaining harmonic signature is rapidly attenuated in amplitude being a result of the roll-off imposed by the low-pass digital filtering specifications. Furthermore, white noise resulted from quantisation process is minimised. It should be noticed that the effective ADC conversion noise floor is not given by the DFT noise floor. Therefore, DFT processing has to be subtracted from the power spectrum figures [38]. For the heart rate measurement only the periodicity of the AC term is relevant. A high pass digital filter guarantees that the slow exponential decay of the PPG signals is completely removed. The discrete structure is configured with the stopband corner frequency set at 0.20 Hz while the lower passband frequency is 0.80Hz.

The DC tracker blocks in Fig. 3 determine the photocurrent DC level for each PPG signal. Consequently, data are collected and passed through a first-order IIR digital integrator. A trapezoidal rule time-domain integration

approximation is chosen due to the property of showing linear phase similar to an ideal digital frequency response [38]. The transfer function is defined by:

$$H_{Tr}(z) = \frac{T_s}{2}\left(\frac{1+z^{-1}}{1-z^{-1}}\right) \tag{8}$$

where T_s is the sampling period.

Finally, a moving average filter (MAF) is the last signal processing function to be applied. Both the quantities, that is, the HR and SpO_2 outputs are smoothed in order to limit any glitch that could jeopardise the results over the last computed estimations. For such purpose, each most recent result is averaged with the last 5 SpO_2 calculations. Since the number of samples used for this operations is fixed by a window length T_w, its frequency-dependent attenuation characteristic has no impact if the MAF averages a short series of time-domain results. Therefore, the MAF keeps a fast transient response. The Z-domain based discrete representation as follows [39]:

$$H_{MAF}(z) = \frac{1}{N}\left(\frac{1-z^{-N}}{1-z^{-1}}\right) \tag{9}$$

and where N is:

$$N = \frac{T_w}{T_s} \tag{10}$$

5. Implementation and Experimental Characterization

5.1. Prototype main components

The oximeter prototype comprises a 32-bit MCU, the MAX30100 SoC and two external power management units that supply 1.8V and 3.3 voltage rails. The digital signal processing tasks for limiting wideband noise and to confine the sampled PPG signals to the bandwidth of interest are performed by a TM4C123 series MCU from Texas Instruments. Fig. 6 depicts the main components of the prototype board.

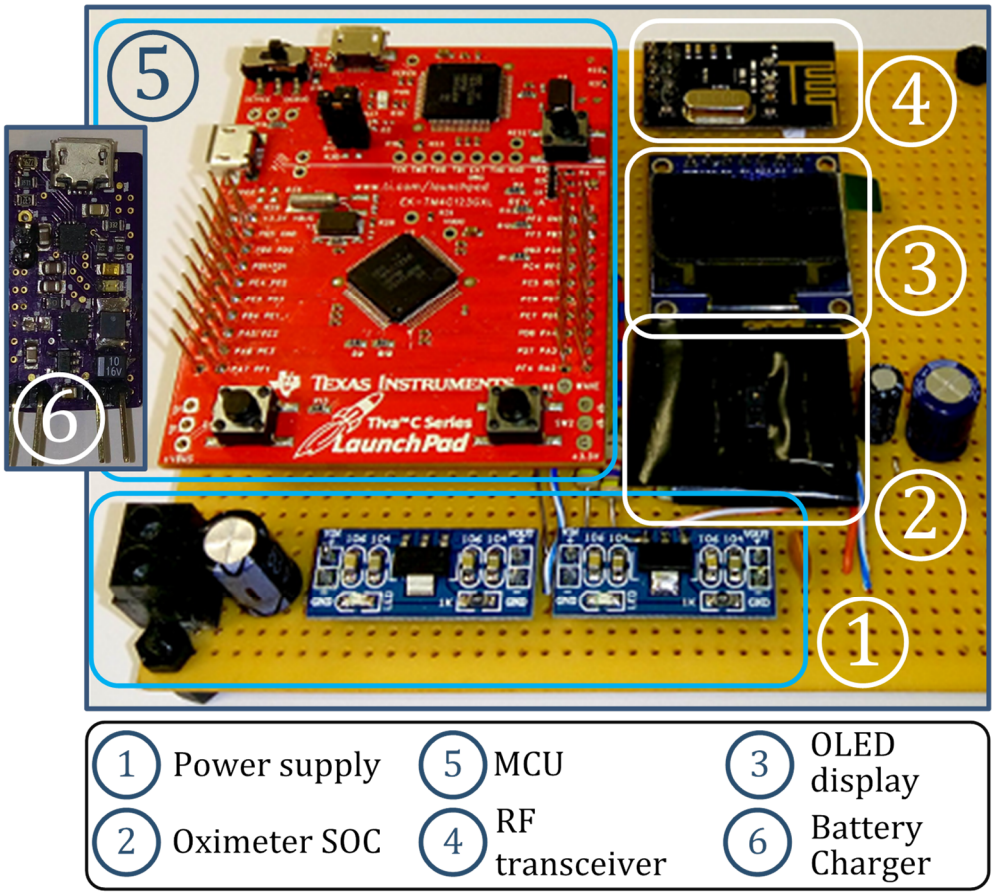

Fig. 6. Reflectance pulse oximeter test board.

Raw and post-processed photo-detector readings along with the SpO_2 and HR estimations are sent to an application developed in Matlab environment. The Matlab operated graphical user interface (MGUI) allows an easy configuration since the MAX30100 SoC has varying number of parameters for its internal operation. The data received by MGUI is acquired in real time through the MCU I2C interface that acts as a virtual com port. Oscilograms of the raw PPGs or post-filtered can be visualised during the tests, enabling the crossing of data being acquired. A general view of the MGUI can be seen in Fig. 7.

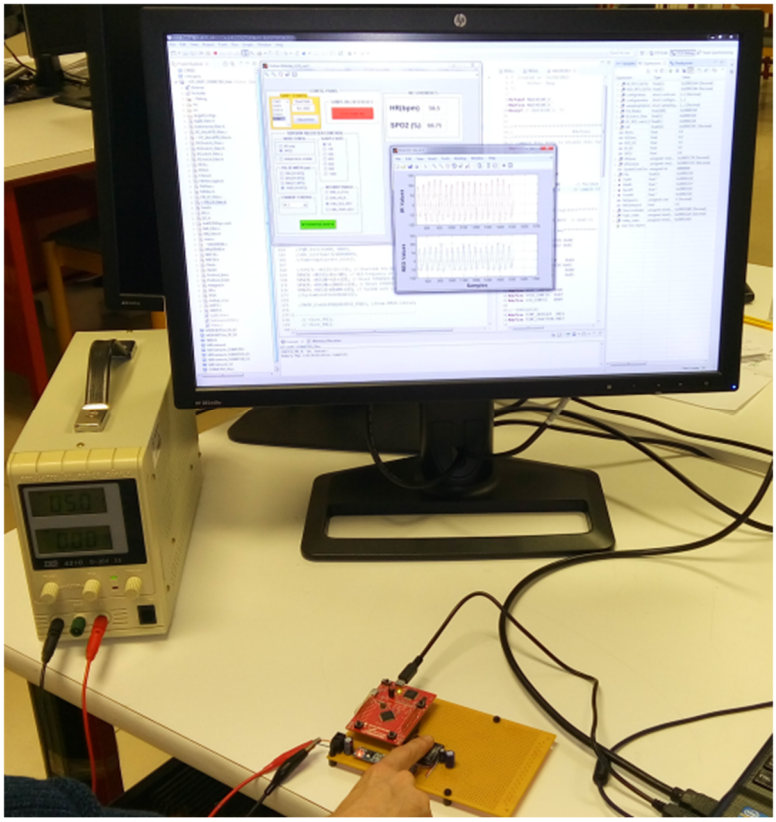

Fig. 7. Prototype board in operation sending real time data to MGUI application.

5.2. Practical results

A. Methodology

With the purpose of verifying the performance of the oximetry system based on the commercial SoC additional software for acquiring and processing the PPG signals was developed. Raw and post-processed readings along with the SpO_2 and HR estimations are sent to an application developed in Matlab environment. The Matlab operated graphical user interface (MGUI) allows an easy configuration since the MAX30100 SoC has varying number of parameters for its internal operation. The data received by MGUI is acquired in real time through the MCU I2C interface that acts as a virtual com port. Oscilograms of the raw PPGs or post-filtered can be visualised during the tests, enabling the crossing of data being acquired. A general view of the MGUI can be seen in Fig. 7.

In order to establish performance marks several tests have been conducted. The physiological signal acquisition from the SoC is extracted through the MCU and then analysed with the use of Matlab. The analysis is performed configuring the SoC with two distinct ADC resolutions. Since the choice of ADC resolution defines the measurement dynamic range, the maximum and minimum resolution available are used as the basis for the evaluation process. In full ADC resolution the system is capable of resolving the PPGs acquisition up to 16-bit. As for the minimum resolution the delta-sigma based ADC ensures no more than 13-bit. In both acquisition modes the sampling rate is identical and set at 50 sps. To select an ADC resolution mode, the SoC internal control imposes specific LEDs on Time. A 1600us pulse width enables 16-bit of resolution while a shorter pulse width of 200us provides 13-bit. Intermediate ADC resolutions are available. However, the authors consider that testing the SoC operation with ADC resolution modes can be a reasonable approach to conduct a summary evaluation of the experimental board performance. In turn, in each one of this ADC operating mode the noise oximeter sensitivity is measured over a set of LEDs driving currents. The tests are organized in three main phases. The first one reveals the PPGs time series in raw format and after being high pass filtered to draw attention to the AC portion. Next, PPG signal quality is estimated for the AC term. Finally, power consumption is measured taking into account

different operating scenarios mentioned above. In addition, a simple metrics is proposed and used to characterize the SoC power consumption versus AC term resolution trade-off. It should be noticed that at this phase of development, the experimental characterisation is confined to fingertip based measurements by the reason of being a body area where the arterial supply is significant. A single subject was used for the test. Several readings were taken considering a time window of 1 minute.

B. PPGs acquisition with 16-bit resolution

The following Figs. 8 to 11 illustrate the PPGs waveforms acquired with the SoC's ADC. The data shown are raw measurements of the sampled photocurrent. Using maximum ADC resolution, the readings are not particularly noisy. However, its presence become more visible as the LEDs current is reduced. The slow exponential decay of the PPG signals has a higher average value when driving LEDs light sources at its maximum current (50mA). In the opposite direction, measurements using progressively lower LEDs pulse currents will result in low AC values. Lowering the LEDs current, the photocurrent detected becomes noisier. From a SNR view point readings are resolved with lesser granularity due to electronic noise generated inside SoC's AFE when driving the LEDs with reduced currents. On the other hand, it should be noticed that a higher LEDs current may relief the low-pass digital filtering requirements inside MCU since the AFE chain and ADC noise sources contribution to PPGs corruption is minimal.

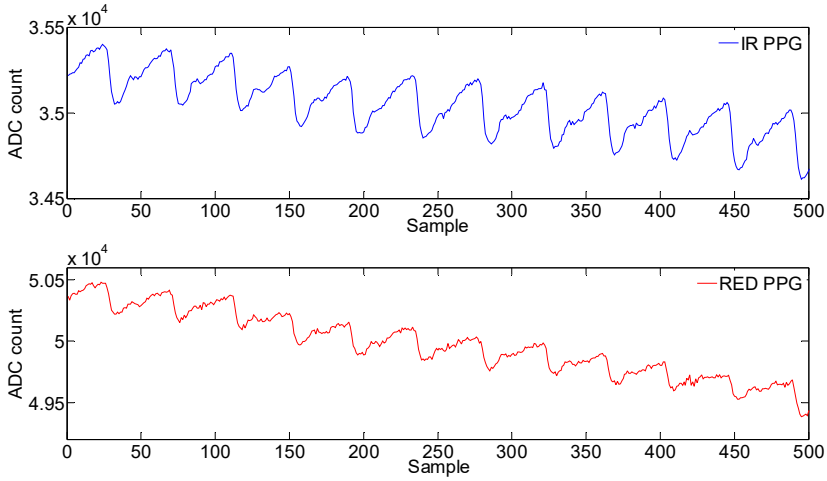

Fig. 8. Raw PPGs obtained with LEDs peak current set to 50mA.

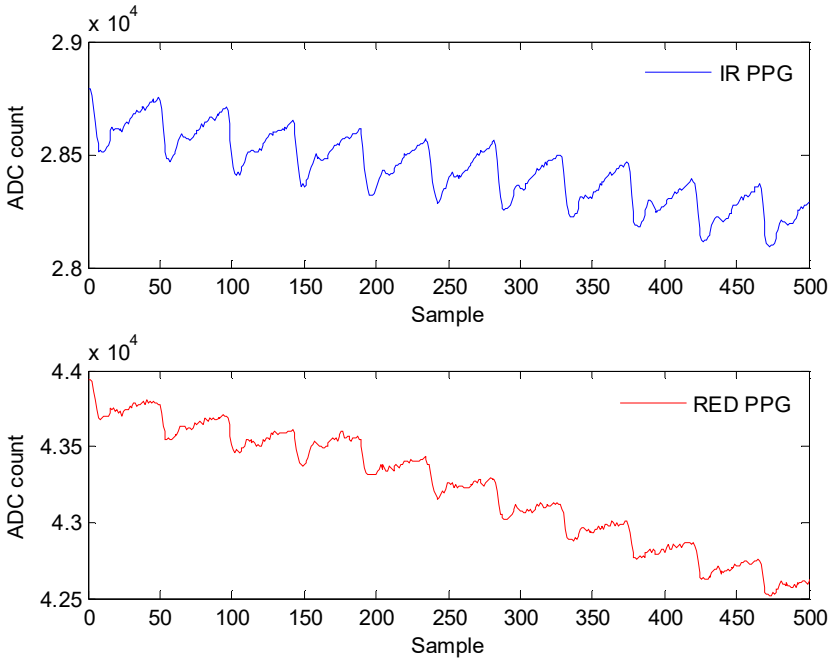

Fig. 9. Raw PPGs obtained with LEDs peak current set to 40.2mA.

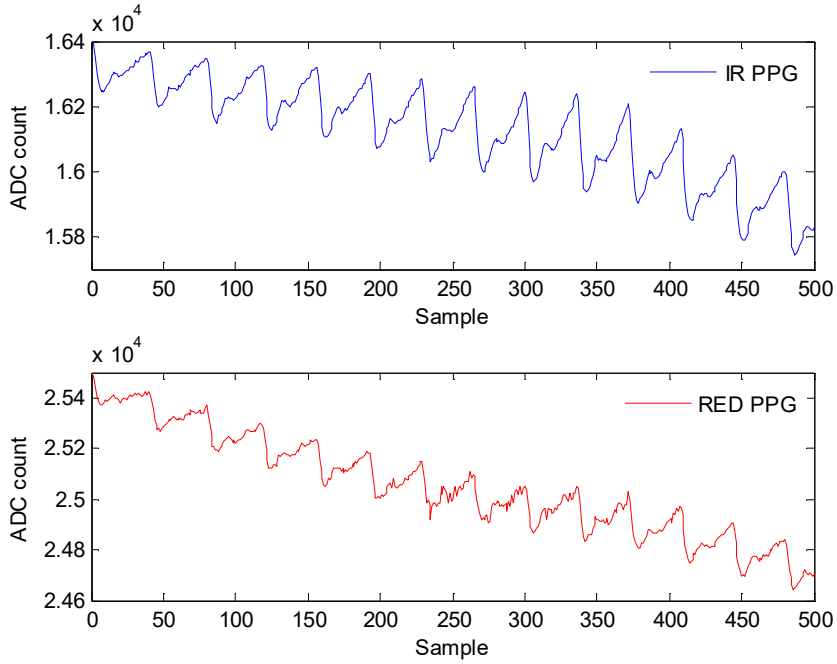

Fig. 10. Raw PPGs obtained with LEDs peak current set to 20.8mA.

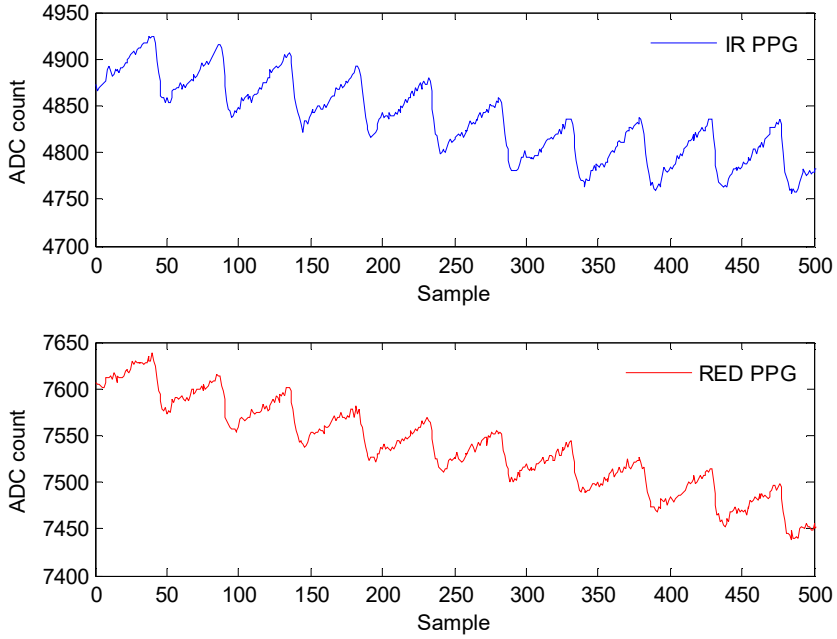

Fig. 11. Raw PPGs obtained with LEDs peak current set to 7.6mA.

Figs. 12-15 show the high pass digital filter based post-processing result for the extraction of the PPGs AC portion. The Figs. 12-15 report the effect of the LEDs pulse current value over the AC amplitude. This procedure is carried out in real time inside the MCU. However, previously, the wide band noise is removed from the incoming raw PPGs. As can be seen in the set of Figs. 12-15 the AC amplitude grows as the LEDs current rises from 7.6mA to 50 mA. By computing the ratio between the pulsatile AC component and DC term based on ADC count numbers (R_{IR} and R_{RED}) the IR PPGs generated ratio value is approximately the double of the ratio calculated with the RED PPG signals. As for the RED channel, the AC term correspond to 0.68%-0.72% of the DC component. The IR PPG signals AC component fraction stands between 0.96%-1.5% of the respective DC component.

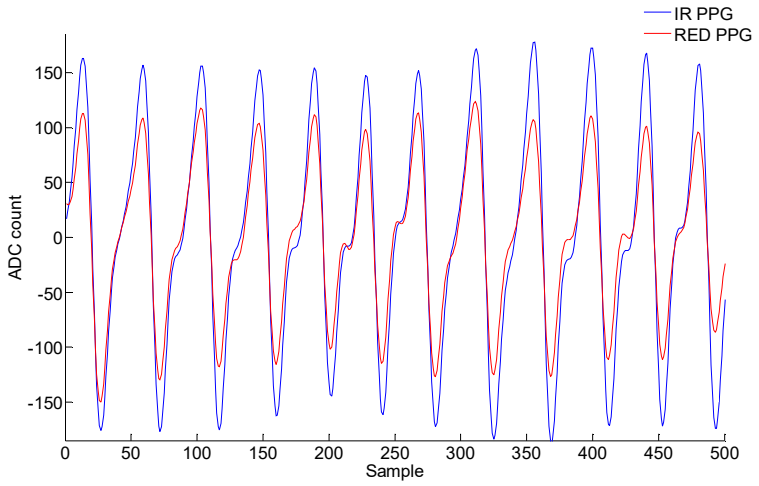

Fig. 12. Filtered PPG AC signals obtained with LEDs peak current set to 50mA.

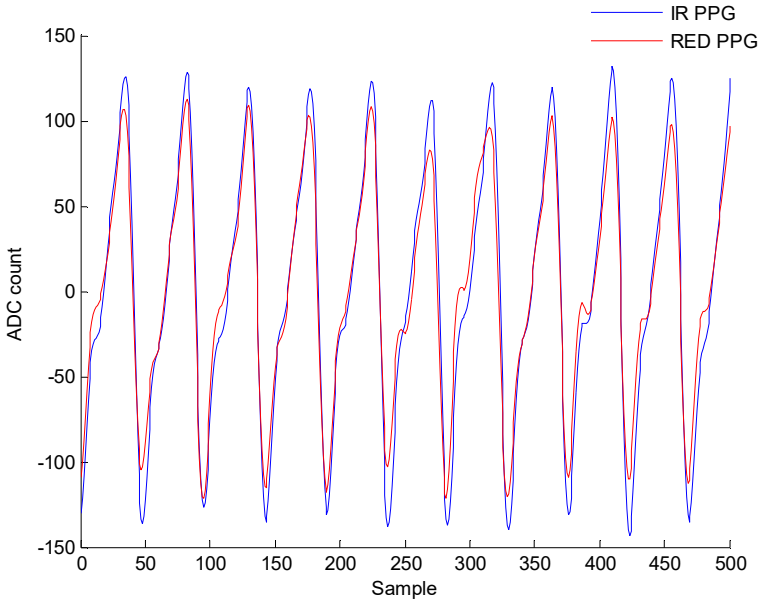

Fig. 13. Filtered PPG AC signals obtained with LEDs peak current set to 40.2mA.

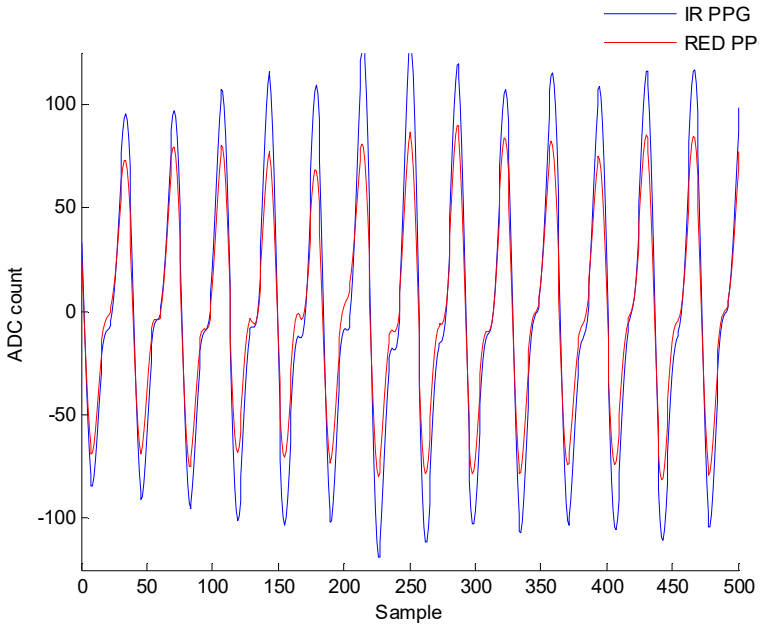

Fig. 14. Filtered PPG AC signals obtained with LEDs peak current set to 20.8mA.

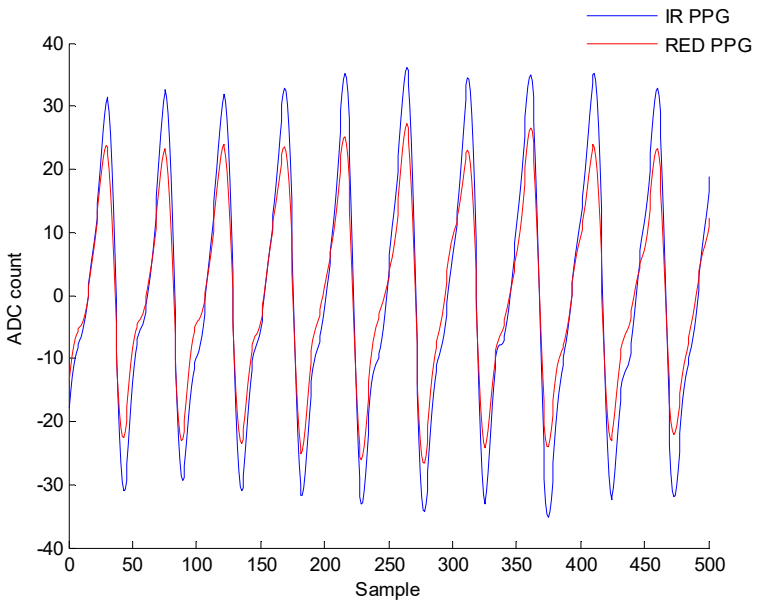

Fig. 15. Filtered AC signals obtained with LEDs peak current set to 7.6mA.

C. PPG acquisitions with 13-bit resolution

The 13-bit resolution raw PPG readings are less clean due to the noise as can be observed in Figs. 16, 17, 18 and 19. Furthermore, signal quality soon becomes degraded as the LEDs are pulsated at lower currents. In fact, at the lowest LEDs current setting is not possible to identify anymore a periodic signal since it is buried in noise (see Fig. 19). Even reinforcing the low pass filter requirements in order to eliminate most of noise outside of the PPG signal frequencies of interest (cut-off frequency of 3Hz) may not be effective since the SNR of the resulting signal will be low.

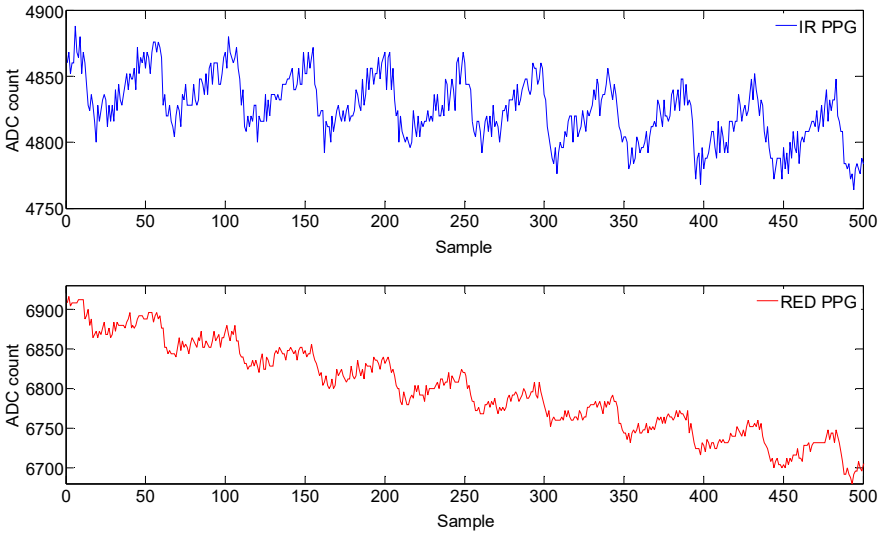

Fig. 16. Raw PPGs obtained with LEDs peak current set to 50mA.

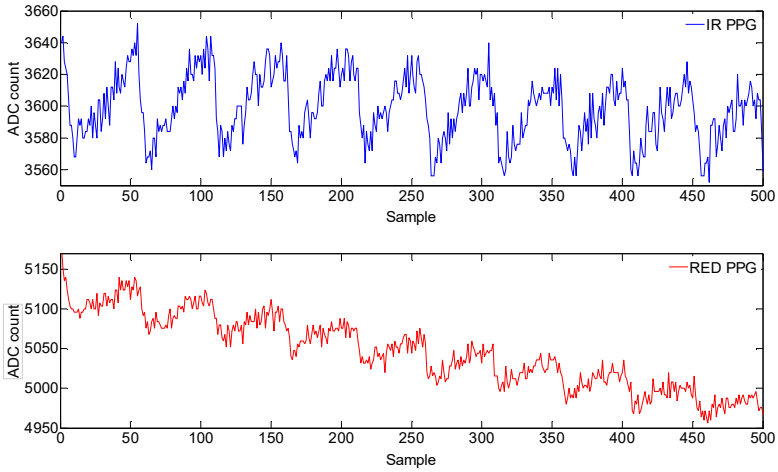

Fig. 17. Raw PPGs obtained with LEDs peak current set to 40.2mA.

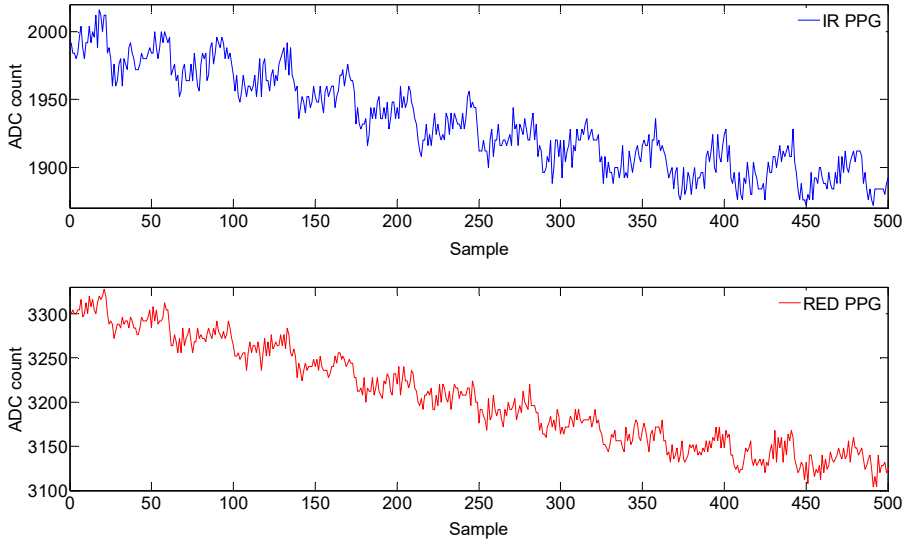

Fig. 18. Raw PPGs obtained with LEDs peak current set to 20.8mA.

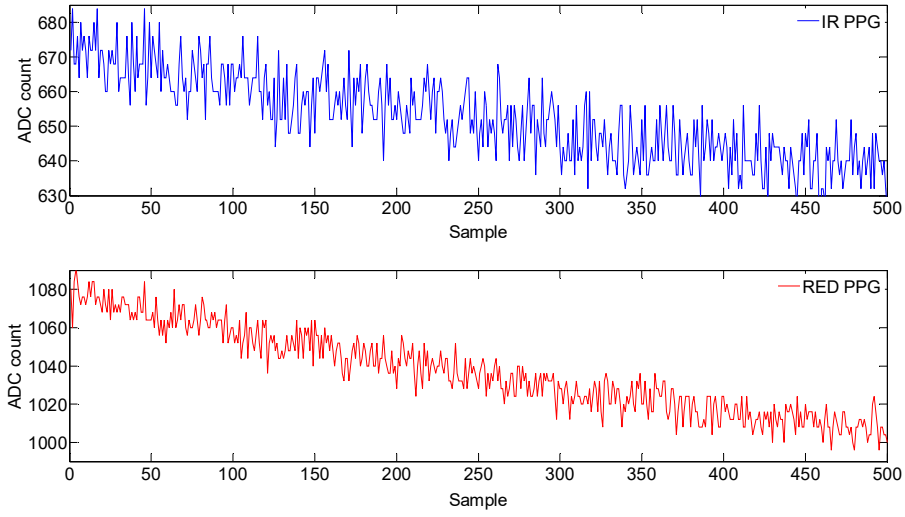

Fig. 19. Raw PPGs obtained with LEDs peak current set to 7.6mA.

While for the PPG AC values Figs. 20, 21, 22 and 23 reveal that in this range of LEDs currents, the ADC output for IR signal AC term codification stands between 35 and 80 ADC counts. Likewise, RED signal AC portion is represented between 30 and 50 counts. The magnitude of the PPG pulsating term is 1.44%-1.85% of the DC

component for the IR PPG readings. In turn, the signal measured by the photodetector with regards to reflected RED light source, the RRED, ranges from 0.75% to 1.07%.

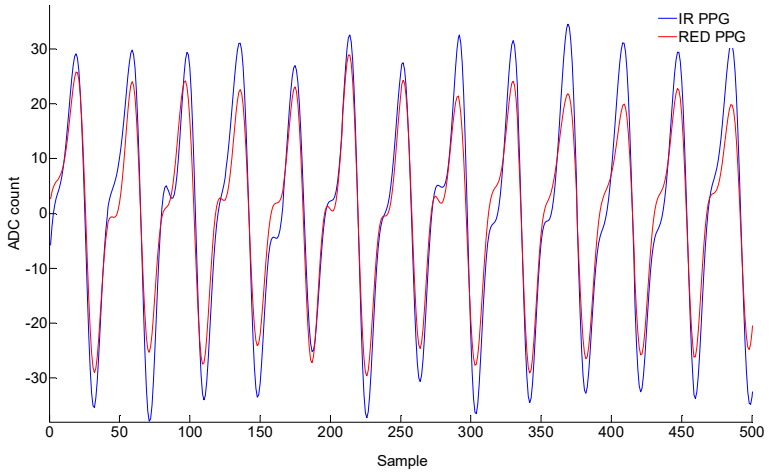

Fig. 20. Filtered PPG AC signals obtained with LEDs peak current set to 50mA

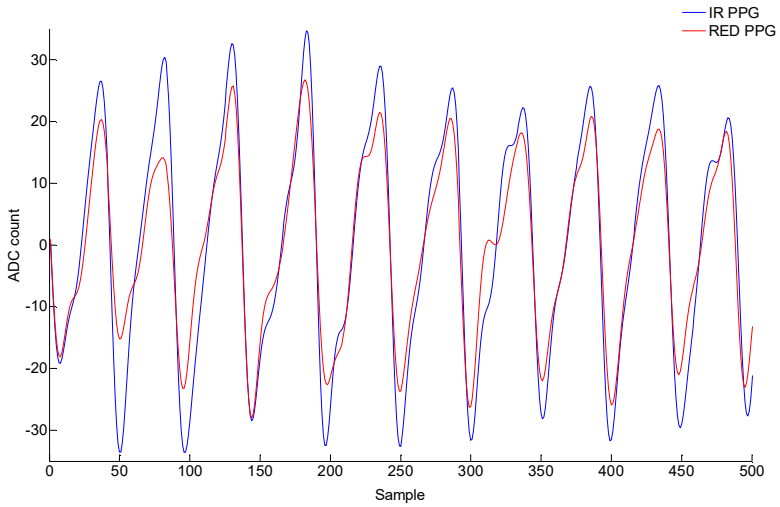

Fig. 21. Filtered PPG AC signals obtained with LEDs peak current set to 40.2mA.

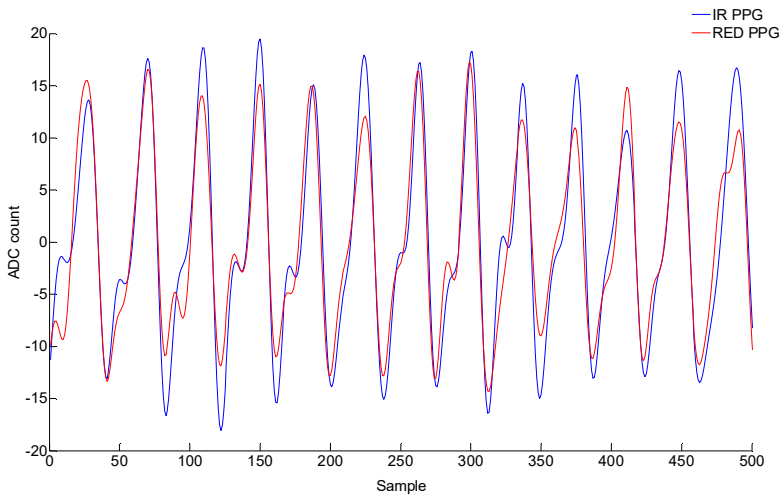

Fig. 22. Filtered PPG AC signals obtained with LEDs peak current set to 20.8mA.

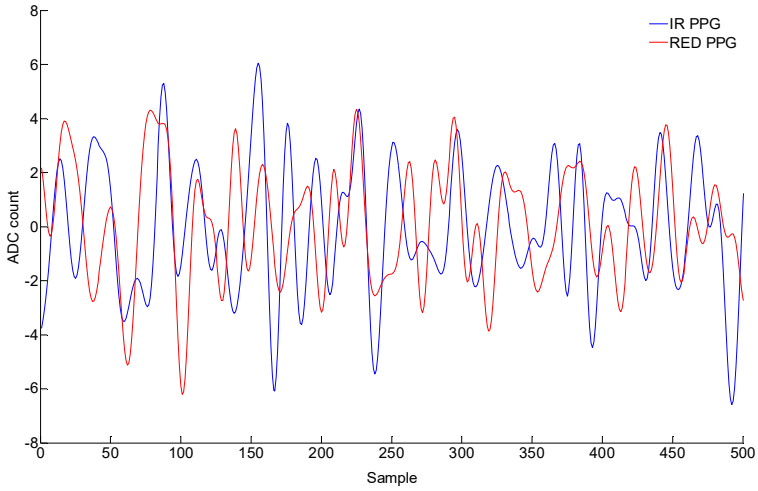

Fig. 23. Filtered PPG AC signals obtained with LEDs peak current set to 7.6mA.

D. Signal quality measurement results

Internal-circuit-generated and external noise limits the readings resolution which is normally expressed through the SNR number [40]. Thus, PPGs data are corrupted by noise. The signal degradation comes from different sources. The most significant comes from the AFE design itself [41]. Other forms of signal quality interference reside on external causes which are the measurement system physical implementation and the subject biological characteristics (subject's skin tone, measurement location or even the applied pressure to the skin). The main challenge for accurate S_pO_2 measurements comes from the fact that the AC component is much lower than the PPG signal DC part. Then, the extraction of the AC portion is a measurement challenge for the instrumentation of acquisition of the signal point of view.

The AC signal level was investigated by splitting the sampled PPGs DC part through a digital filter. The peak-to-peak AC part was converted to an equivalent N-bit resolution converter. Tables I and II represent the DC component average amplitude scaled to number of bits with regards to the ADC resolution. These numbers were recorded for a range of LEDs currents starting at 4.4mA and ending at 50mA. Using the SoC's maximum ADC resolution the AC term is codified with circa 8 bits at a maximum LEDs current while a minimum of 5 bits is obtained driving the LEDs at lowest level of current as documented in Table I. In turn, at a minimum resolution of 13 bits the bit representation based amplitude goes from 4.7 bits to circa 6 bits for LEDs currents between 17.4mA and 50 mA. For the lowest testing currents (4.4 mA and 7.6mA) it wasn't possible to get consistent results since the noise level is too high.

TABLE 1. 16-BIT SAMPLE ACQUISITION

I_{LED} (mA)	IR PPG AC portion (digitization levels)	Digital code length (bits)	RED PPG AC portion (digitization levels)	Digital code length (bits)
50	241,8	7,9	179,1	7,5
40,2	210,5	7,7	171,8	7,4
27,1	194,7	7,6	139,4	7,1
17,4	147,9	7,2	100,0	6,6
7,6	73,5	6,2	49,6	5,6
4,4	31,2	5,0	23,2	4,5

TABLE 2. 13-BIT SAMPLE ACQUISITION

I_{LED} (mA)	IR PPG AC portion (digitization levels)	Digital code length (bits)	RED PPG AC portion (digitization levels)	Digital code length (bits)
50	51,1	5,7	37,2	5,5
40,2	51,5	5,7	44,1	5,5
27,1	33,0	5,0	25,0	4,6
17,4	25,7	4,7	16,9	4,1
7,6	-	-	-	-
4,4	-	-	-	-

E. Power consumption characterization

A wearable device should be carefully designed to minimise the power consumption. Modern electronics development is driven by low energy needs. From this point of view and combining different power management techniques an oximeter design can achieve very reduced power consumption numbers. However, the overall energy balance is determined by the operation of the IR and RED LED units. Which is to say, the LEDs light intensity and the on time period are what really penalises the power consumption.

In this regard, electrical measurements were performed to ascertain the LEDs current along with the PPG sample acquisition impact on SoC power consumption. The device was programmed to acquire the PPG samples with 16-bit and 13- bit resolution over different LEDs light intensity driven by different current values. The set of measurements is divided into two groups. The measurements form the first group are current waveforms acquired through an oscilloscope. The second group of data are power consumption calculations obtained from simultaneous voltage and current readings. For these readings a measurement device with 12-bit of resolution was used. All power consumptions records represent average values over a time window of 1 s.

Figs. 24 and 25 depict SoC current waveforms. Fig. 24 reveals the current variation with SoC's ADC working at 16-bit while the Fig. 25 relates to the operation of the ADC at 13-bit. In both modes PPGs are sampled at 50 sps with IR and RED LEDs driven at maximum current (50mA). The trace 1 is the signal generated by the SoC when new PPG digital signals are ready to be processed by the MCU. The trace 2 is the current measured at SoC's input which includes the LEDs consumption. A precision current sensing circuit was built for this purpose. The trace 3 is the shunt current monitor output divided by the measurement circuit gain (60V/V). That is to say, the current signal represented by the trace 2 can be analysed directly in mA (1mV=1mA). Electrical current maximum and minimum and average values can be consulted in the right column in the Figs. 24 and 25. During LEDs' off time the SoC's electrical consumption is low – circa 1.5 mA. But from average current analysis point of view enabling maximum resolution ADC conversion requires almost four times more average current than with minimum ADC resolution. This difference is explained by the fact that the LEDs current pulse width is 1.6ms to get SoC's maximum ADC resolution. In its turn, getting PPGs with 13-bit of resolution LEDs current pulse width is 200µs which is 8 times smaller than what is needed for acquiring 16-bit samples. The on time period in any case is set by the SoC.

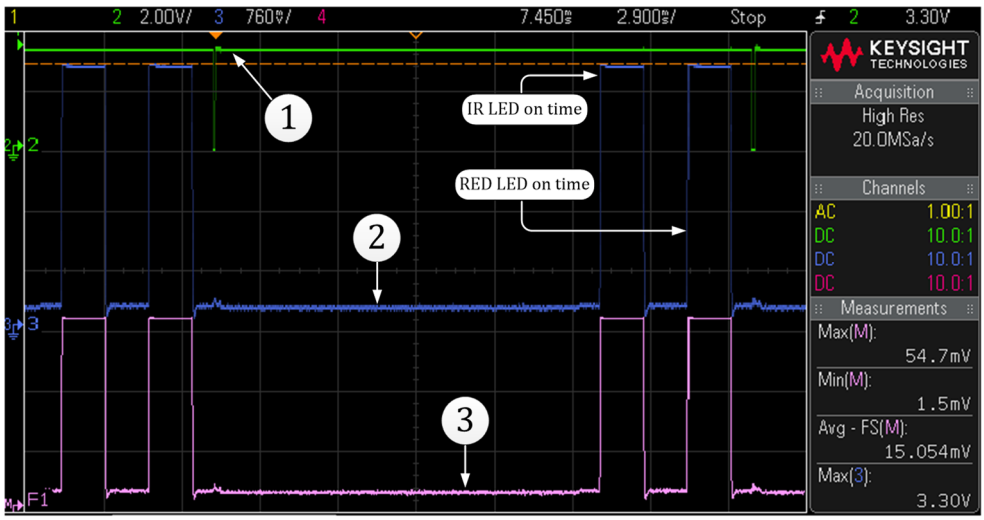

Fig. 24. SoC operation with 16-bit samples acquisition: 1) ADC end of conversion signal; 2) Current sensor output; 3) Current sensor output divided by the measurement gain.

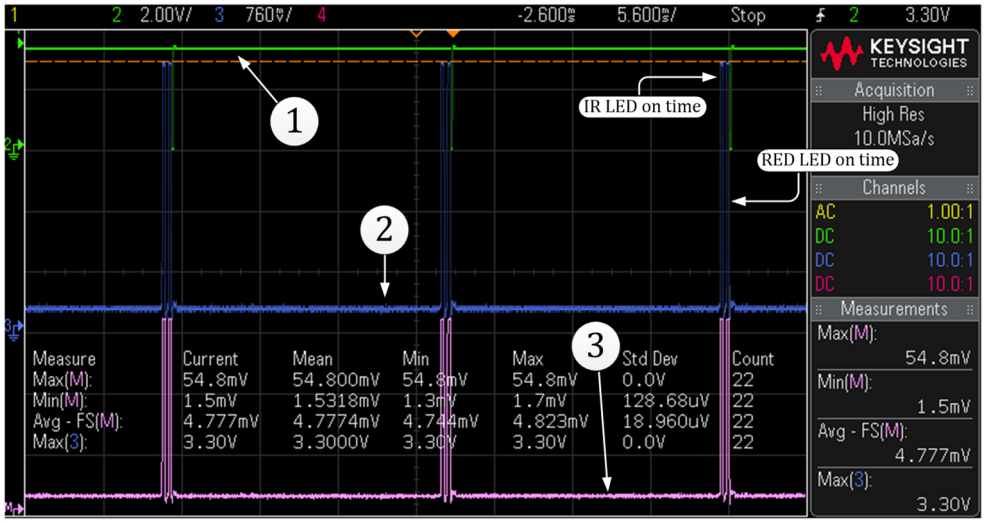

Fig. 25. SoC operation with 16-bit samples acquisition: 1) ADC end of conversion signal; 2) Current sensor output; 3) Current sensor output divided by the measurement gain.

Fig. 26 shows the MCU current consumption over 50 ms. The trace 1 is the MCU current. The trace 2 is the same current signal obtained through the shunt current sensor but now divided by the measurement circuit gain. The waveform presents a periodic current peak which corresponds to the processing of sampled PPG signals inside MCU. Furthermore, the duration of these events is due to the post-processing numerical calculations needed to clean up the fresh PPGs samples and to extract its AC component.

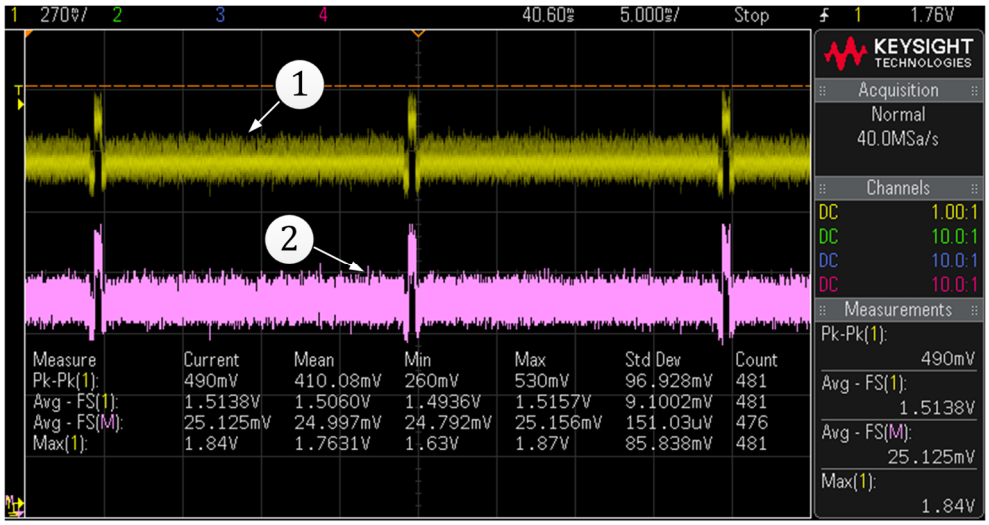

Fig. 26. MCU operation: 1) Current sensor output; 2) Current sensor output divided by the measurement gain;

To analyse the power consumption of the SoC system the RED and IR LEDs are driven with a set of currents (4.4mA, 7.6mA, 17.4mA, 27.1mA, 40.2mA and 50 mA). Several combinations of LEDs light intensity and on-time duration are available. However, the combinations are not selected at will. They are imposed by the SoC according to the required ADC resolution. This means high resolution digitization comes at expense of higher energy consumption while a lower resolution conversion process is less demanding. In this regard, a fully characterization of SoC power consumption can be made comparing the two opposing extremes of the ADC resolutions. To have a fair comparison both measurements were performed at the same sampling rate (50 sps). Fig. 27 shows the power consumption numbers resulting from the acquisition of the PPG samples at 13-bit and 16-bit resolution. At minimum LEDs light intensity the average power does not differ significantly. As soon as the LEDs light intensity is increased the power required to get maximum ADC resolution grows much faster. At maximum LEDs current the power needs has more than doubled, but for the 13-bit conversation mode the rising rate of power consumption is nearly null. Moreover, a peculiar fact can be observed in the power consumption evolution regarding the PPGs acquisition with 16-bit of resolution - the power solicitation in the range from 40 mA to 50 mA is almost constant.

The increasing gap between the two power traces has to do with the current pulse on-time duration already discussed. The current waveforms documented in Fig. 25 and Fig. 26 support this conclusion.

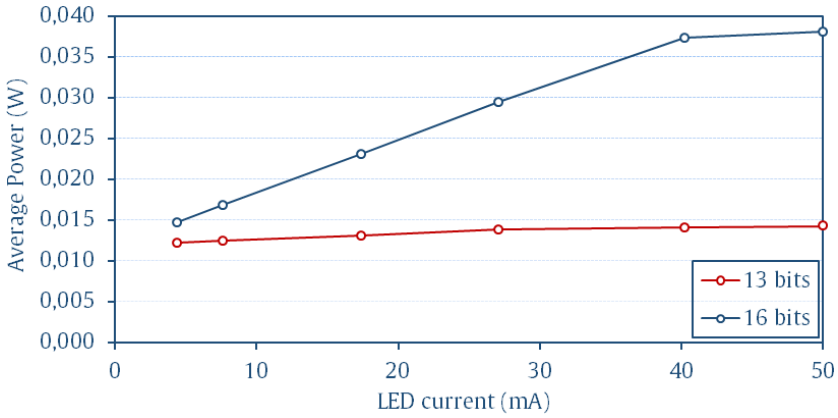

Fig. 27. SoC average power measured in the full range of LEDs current settings.

F. *Signal quality and power consumption trade-off*

High fidelity PPGs depend on the LEDs on time and current value. However, designing a wearable device to be conservative in terms of energy consumption in order to increase the battery life comes at the expense of signal quality. Therefore, it is a matter of trade-off between these two requirements. In this sense, it is proposed a novel metric that enables a trade-off analysis between the SoC power consumption and the required signal quality. Here, signal quality should be interpreted as the number of bits used to code the PPGs AC term peak-to-peak amplitude. The digital code extraction was presented and discussed in section 5.2.D. This metric establishes a relation between the power consumption and PPG signal quality outcomes in the form of a ratio. The idea is to provide a simple and yet effective tool to characterize the design measurement system sensibility towards the power consumption required to get a certain signal quality. This approach can be useful, for example, to evaluate a preliminary design at first stages of development. That is to say, the design can be modified and consequently verified if the changes are in line with a specified compromise previously established. However, in the present paper the goal is only to introduce the metric and show its effectiveness with the real data based on the developed prototype.

The power to signal ratio (PSR) are formulated for both PPG variables as:

$$PSR_{IR} = \frac{P_{SoC}^{AVG}}{AC_{IR}^{ENB}} \tag{11}$$

and

$$PSR_{RED} = \frac{P_{SoC}^{AVG}}{AC_{RED}^{ENB}} \tag{12}$$

where AC_X^{ENB} is the AC component peak to peak value in ADC bits and P_{SOC}^{AVG} represents the average power required by the SoC internal blocks (signal processing modules together with the LEDs power circuit).

For the experimental evaluation the same set of LEDs driving currents was used. Input data were acquired with 13 and 16-bit resolution. The PSR outcomes are shown in Figs. 28 and 29. Observing the Fig. 28 it can be noticed that the PSR values highlight a mismatch between the two PSR curves due to the reason of a slight discrepancy between the light intensity of the two LEDs. Despite both LEDs being controlled with the same maximum reference current, a slight lower level of current in the RED LED was measured. In practice, the difference in relation to the IR LED is circa 5mA. In Fig. 28 the PSR curves highlight three distinct regions. Two of them reveal constant PSR which are at the extreme limits of the current scale while a third shows a linear grow. The rapid growth of the PSR in the intermediate LEDs current values is a clear sign that the signal quality enhancement has a slower rate compared with the power consumption and, as a consequence, the ratio increases. The location of a minimum PSR does not coincide with the LEDs being driven with the lowest testing current. In fact, the minimum registration occurs at 7.6mA. From the ratio point of view this LEDs current value should be chosen if the design goal is to minimize the

energy consumption and at the same time preserving enough signal quality. As seen in the Table 2, in case of the LEDs powered with a current intensity of 7.6mA the signal quality loses circa 1.9 bits of resolution relative to what is possible to get at maximum current of 50mA. That is, choosing the LEDs current of 7.6mA expected power consumption is less than 3mW for each bit of resolution used to represent the PPG AC amplitude. In contrast, operating the LEDs with the maximum allowed current the ratio jumps to circa 5mW/AC_{bit}. In sum, potential energy savings exceeds 40% if the loss of resolution bits is acceptable. However, if the objective is to guarantee a higher level of signal quality, it is unlikely to obtain such performance at lowest values of the current scale. On the other hand, the PSR plot shows unequivocally that the two highest LEDs currents produce almost the same PSR. In this respect, does not make sense to choose the current reference of 50 mA. Therefore, the PSR plot has helped to make a decision that could reduce the power consumption without significantly affecting the signal quality.

In Fig. 29 the PSR values show a magnitude variation that is circa 0.5mW/AC_{bit} of the full scale. Although the difference is residual among the LEDs current references, the obtained PSR data reveals a curve that facilitates the analysis and consequently the choice. As the LEDs current is incremented the signal quality grows faster than the power consumption. Thus, the PSR tends do decrease allowing to facilitate the decision. That is, the minimum ratio is provided with a LEDs current of 40.2mA.

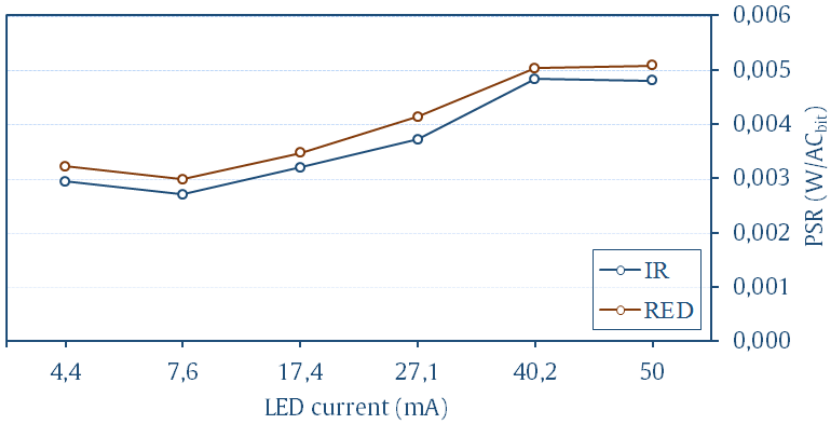

Fig. 28. PSR vs LEDs current (16-bit resolution samples).

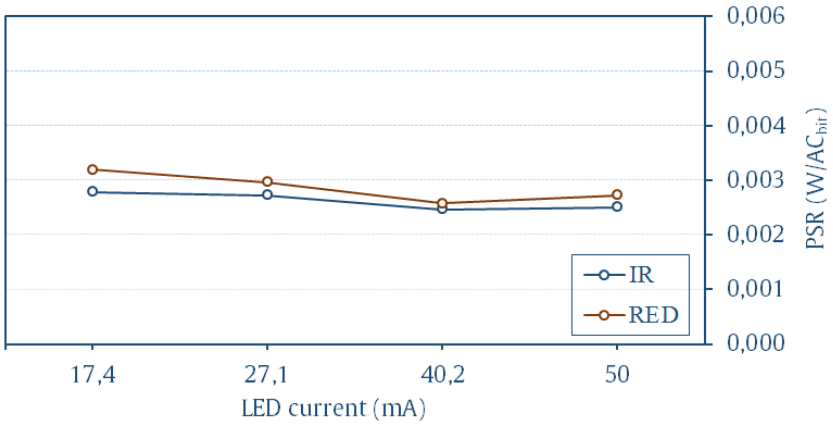

Fig. 29. PSR vs LEDs current (13-bit resolution samples).

5.3. Discussion and limitations of the study

In [11], an ultra-low power oximeter is proposed unveiling an extremely minimum power consumption of 4.8mW and compared to a set of low power commercial pulse oximeters, which revealed having a significantly higher consumption. In turn, our developed prototype has higher power consumption, but significantly lower if compared with the power measurements obtained with respect to the commercial units. According to our experimental tests, the prototype power consumption does not exceed 40mW at a maximum LED current of 50mA for an acquisition at 16-bit of resolution, which is approximately 10% lower to the lowest power reading among the commercial pulse oximeters. In this sense, the developed prototype reveals a better power consumption

performance than the commercial solutions presented in [11]. However, a close comparison in the context above is meaningless without the provision of an associate signal quality figure. In this regard, [13] reported SNR estimations regarding SpO_2 measurements from an AFE side design perspective while investigating the power consumption. Our prototype design has shown that high signal quality measurements cannot be obtained just using the lowest LED currents. While the signal quality results coming from our prototype are to some extent comparable to [13], they are attained at the expense of higher power consumption. In terms of the literature focused in the research of pulse oximetry aiming on the signal measurement chain optimisation, several studies rely on ADC 12-bit and 24-bit. The authors consider that 12-bit is not enough to be able to extract the PPG AC component since the levels of digitalization are limited [3], [7]. On the other hand, other studies use the 24-bit ADC that grants an enhanced sensibility of the measurement of physiological signals [34] [42]. However, opting to design the oximeter with 24-bit will be translated in an increased cost and occupied space, which compromises the objective of creating a wearable solution of low cost and low power. Thus, the authors consider the SoC utilised in this paper is an acceptable solution, since it is a compact solution in terms of space, offering readings with a reasonable ADC resolution of 16-bit and with moderate energy consumption.

The present study presents some limitations. For instance, the accuracy of the experimental pulse oximeter was not possible to be determined. In order to define it, it would require an arterial blood gas analyser (SaO_2) for comparing with SpO_2 readings provided by the prototype. In this regard, the procedure for the determination of the prototype metrological performance can be based on estimating the accuracy root mean square (ARMS) parameter, which describes the devices general performance over the entire saturation range [43]. In addition, it is not recommended for a serious in-depth metrological study to limit the comparison to just one co-oximeter. Therefore, for a validation study, multiple co-oximeters are normally employed according to the literature [42]. However, another alternative solution could be employed by comparing it to commercial pulse oximeters used in a clinical environment. The final option could be to use commercially available instruments to recreate the human finger optical properties and, in this way, to calibrate the relation between R with SpO_2. This method provides a cost-effective approach compared to the aforementioned solutions. However, only three simulated arterial oxygen saturation levels are available (80%, 90% and 97%) [11]. In contrast with the other two approaches, it is possible to measure dozens or hundreds of points over the range of 70%-100%. Moreover, the impact of motion artefacts on SpO_2 readings was not addressed in this paper, since this requires an in-depth study regarding post-processing techniques. Several methods for detection and reduction of motion artefacts have been published over the years [44], [45] and [46]. However, adequate robustness to these phenomena is of particular importance, as the wearable pulse oximeter is aimed at a daily use where the subject movement is unavoidable.

6. Conclusion

This paper has presented an oximeter design based on a high integrated SoC which combines a dedicated AFE circuitry connected to a 16-bit delta-sigma ADC for PPGs acquisition. The sensing device measured PPGs by reflective pulse oximetry principle as an alternative to transmission pulse technique. Several post-processing techniques were implemented in order to enhance PPG signal quality. In this regard, a design concept is discussed in detail and a complete prototype was built which was evaluated by experimental characterization. Since the developed sensor for wearable health has a significant number of settings that enables different operating conditions, finding out the impact on global performance was one of the research goals of the paper. In this sense, a set of tests aiming the evaluation of two main key features (power consumption performance and signal quality) were performed which are critical for wearable health monitoring applications.

The DC and pulsatile AC components sensitivity of the PPG signals to different LEDs current values (7.6mA - 50 mA) were investigated for the highest and lowest ADC resolutions (16-bit and 13-bit) with a sample rate of 50sps. The raw 16-bit PPGs samples showed to be less noisy in comparison with the 13-bit PPG samples, meaning that the post-digital filtering requirements for 16-bit acquisitions are looser. It was verified that the ratio between the IR PPGs pulsatile AC component and DC term is around two times the ratio provided by the RED PPGs whether the conversion is performed with 16-bit or 13-bit. Therefore, the IR PPG signal was more sensitive in terms of AC component amplitude. Nevertheless, even at the maximum digital resolution the IR PPGs AC quota did not surpass 1.5% of the PPG sample DC portion for a maximum LEDs driving current of 50mA.

The power consumption characterization tests unveiled distinct results. For 13-bit resolution acquisitions increasing LEDs current had minimum effect. That is to say, the average power consumption remains almost constant at circa 14 mW. On the other hand, by jumping to the highest resolution the power necessity of the device more than doubles between 17.4 mA and 50mA of LEDs current, thus reaching around 37mW.

The signal quality was quantified by cutting the sampled PPGs DC part through a digital filter. The AC part peak-to-peak was converted to an equivalent N-bit resolution converter. For PPGs sampled at maximum resolution the AC portion showed a digital representation ranging from 4.5-bit to 7.9-bit resolution. As expected, at the lowest sampling rate the AC component was coded with lower resolution, thus losing circa 2-bit resolution. Furthermore, LEDs currents testing were reduced because the two lowest LEDs driving currents (4.6 mA and 7.6 mA) did not produce consistent results but only pure noise readings.

As for the second research objective, a performance merit figure named as PSR was proposed, which addressed the power consumption and signal quality trade-off issue. The novelty of this metric relies on the fact that the relationship between the power consumption and signal quality can be plotted over different operating conditions given the insights about the oximeter design approach. In this way, PSR local minimums can be identified and analysed in order to find which one offers the best compromise solution regarding measurement sensitive goal. Thus, it can be applied to explore different design configurations during the oximeter development stage. PSR to LEDs current data were collected to determine the effectiveness of the tool based on two set of PPG samples with 16-bit and 13-bit resolution, respectively. The PSR figures obtained from 13-bit samples showed that driving IR and RED LEDs with a high current level among the values tested provided a direct answer by maximising sample signal quality with minimum power consumption. On the other hand, PSR computation derived from 16-bit PPG samples made clear the impossibility of fulfilling the requirement of minimum power with regards to signal quality, since a minimum value for PSR was found using low LEDs currents which penalised the sensitivity of the measurement. However, the same PSR plot pointed out a compromise solution by highlighting that at high LEDs currents levels the PSR numbers are almost equal. Therefore, it is possible to ensure sufficient PPG signal quality with intermediate power consumption. Thus, by using intermediate LEDs current setting it is possible to extract the PPG signals with a considerable signal quality without having to maximize the LEDs current.

Acknowledgments

The authors would like to acknowledge Daniel F. Cruz for his participation in the development of the equipment. Moreover, João P. S. Catalão acknowledges FEDER funding (European Union) through COMPETE and Portuguese funding through FCT, under Projects FCOMP-01-0124-FEDER-020282 (Ref. PTDC/EEA-EEL/118519/2010) and UID/CEC/50021/2013, and also funding from the EU 7th Framework Programme FP7/2007-2013 under grant agreement no. 309048.

References

[1] Y. Li, C. C. Y. Poon and Y.-T. Zhang, "Analog Integrated Circuits Design for Processing," *IEEE Reviews in Biomedical Engineering,* vol. 3, pp. 93-105, 2010.

[2] D. Li, H. Zhao and S. Dou, "A new signal decomposition to estimate breathing rate and heart rate from photoplethysmography signal," *Biomedical Signal Processing and Control,* vol. 19, pp. 89-95, 2015.

[3] K. Li and S. Warren, "A Wireless Reflectance Pulse Oximeter With Digital Baseline Control for Unfiltered Photoplethysmograms," *IEEE Transactions on Biomedical Circuits and Systems,* vol. 6, no. 3, pp. 269-278, 2012.

[4] Y. Zhang, B. Liu and Z. Zhang, "Combining ensemble empirical mode decomposition with spectrum subtraction technique for heart rate monitoring using wrist-type photoplethysmography," *Biomedical Signal Processing and Control,* vol. 21, pp. 119-125, 2015.

[5] M. Khan, C. G. Pretty, A. C. Amies, R. Elliott, Y. S. Chiew, G. M. Shaw and J. G. Chase, "Analysing the effects of cold, normal, and warm digits on transmittance pulse oximetry," *Biomedical Signal Processing and Control,* vol. 26, pp. 34-41, 2016.

[6] J. A. Sukor, M. S. Mohktar, S. J. Redmond and N. H. Lovell, "Signal Quality Measures on Pulse Oximetry and Blood Pressure Signals Acquired from Self-Measurement in a Home Environment," *IEEE Journal of Biomedical and Health Informatics,* vol. 19, no. 1, pp. 102-108, 2015.

[7] R. G. Haahr, S. B. Duun, M. H. Toft, B. Belhage, J. Larsen, K. Birkelund and E. V. Thomsen, "An Electronic Patch for Wearable Health Monitoring by Reflectance Pulse Oximetry," *IEEE Transactions on Biomedical Circuits and Systems,* vol. 6, no. 1, pp. 45-53, 2012.

[8] S. V. Gubbi and B. Amrutur, "Adaptive Pulse Width Control and Sampling for Low Power Pulse Oximetry," *IEEE Transactions on Biomedical Circuits and Systems,* vol. 9, no. 2, pp. 272-283, 2015.

[9] S. B. Duun, R. G. Haahr, K. Birkelund and E. V. Thomsen, "A Ring-Shaped Photodiode Designed for Use in a Reflectance Pulse Oximetry Sensor in Wireless Health Monitoring Applications," *IEEE Sensors Journal,* vol. 10, no. 2, pp. 261-268, 2010.

[10] M. Shokouhian, R. Morling and I. Kale, "Interference Resilient Sigma Delta-Based Pulse Oximeter," *IEEE Transactions on Biomedical Circuits and Systems,* vol. 10, no. 3, pp. 623-631, 2016.

[11] M. Tavakoli, L. Turicchia and R. Sarpeshkar, "An Ultra-Low-Power Pulse Oximeter Implemented With an Energy-Efficient Transimpedance Amplifier," *IEEE Transactions on Biomedical Circuits and Systems,* vol. 4, no. 1, pp. 27-38, 2010.

[12] K. Li, S. Warren and B. Natarajan, "Onboard Tagging for Real-Time Quality Assessment of Photoplethysmograms Acquired by a Wireless Reflectance Pulse Oximeter," *IEEE Transactions on Biomedical Circuits and Systems,* vol. 6, no. 1, pp. 54-63, 2012.

[13] K. Glaros and E. Drakakis, "A Sub-mW Fully-Integrated Pulse Oximeter Front-End," *IEEE Transactions on Biomedical Circuits and Systems,* vol. 7, no. 3, pp. 363-375, 2013.

[14] Y. S. Yan and Y. T. Zhang, "An Efficient Motion-Resistant Method for Wearable Pulse Oximeter," *IEEE Transactions on Information Technology in Biomedicine,* vol. 12, no. 3, pp. 399-405, 2008.

[15] K. H. Chon, S. Dash and K. Ju, "Estimation of Respiratory Rate From Photoplethysmogram Data Using Time–Frequency Spectral Estimation," *IEEE Transactions on Biomedical Engineering,* vol. 56, no. 8, pp. 2054-2063, 2009.

[16] N. Selvaraj, K. H. Shelley, D. G. Silverman, N. Stachenfeld, N. Galante, J. P. Florian, Y. Mendelson and K. H. Chon, "A Novel Approach Using Time–Frequency Analysis of Pulse-Oximeter Data to Detect Progressive Hypovolemia in Spontaneously Breathing Healthy Subjects," *IEEE Transactions on Biomedical Engineering,* vol. 58, no. 8, pp. 2272-2279, 2011.

[17] J. Lee and K. H. Chon, "Time-Varying Autoregressive Model-Based Multiple Modes Particle Filtering Algorithm for Respiratory Rate Extraction From Pulse Oximeter," *IEEE Transactions on Biomedical Engineering,* vol. 58, no. 3, pp. 790-794, 2011.

[18] W. Karlen, S. Raman, J. M. Ansermino and G. A. Dumont, "Multiparameter Respiratory Rate Estimation From the Photoplethysmogram," *IEEE Transactions on Biomedical Engineering,* vol. 60, no. 7, pp. 1946-1953, 2013.

[19] M. R. Ram, K. V. Madhav, E. H. Krishna, N. R. Komalla and K. A. Reddy, "A Novel Approach for Motion Artifact Reduction in PPG Signals Based on AS-LMS Adaptive Filter," *IEEE Transactions on Instrumentation and Measurement,* vol. 61, no. 5, pp. 1445-1457, 2012.

[20] A. Dixit, R. Sharma and S. Barai, "Developing and Prototyping Pulse Oximeter for Elderly People," *Materials Today: Proceedings,* vol. 2, no. 4–5, pp. 1560-1567, 2015.

[21] G. Pang and C. Ma, "A Neo-Reflective Wrist Pulse Oximeter," *IEEE Access,* vol. 2, pp. 1562-1567, 2014.

[22] A. Serteyn, R. Vullings, M. Meftah and J. W. M. Bergmans, "Motion Artifacts in Capacitive ECG Measurements: Reducing the Combined Effect of DC Voltages and Capacitance Changes Using an Injection Signal," *IEEE Transactions on Biomedical Engineering,* vol. 62, no. 1, pp. 264-273, 2015.

[23] O. S. Fathabadi, T. J. Gale, J. Olivier and P. A. Dargaville, "Automated control of inspired oxygen for preterm infants: What we have and what we need," *Biomedical Signal Processing and Control,* vol. 28, pp. 9-18, 2016.

[24] M. Hülsbusch, V. Blazek, M. Herzog, S. Vogel, T. Wartzek, D. Starke and T. Hennig, "Development of a miniaturized in-ear pulse oximeter for long term monitoring of risk patients," in *IFMBE Proceedings World Congress on Medical Physics and Biomedical Engineering*, Munich, Germany, 2009.

[25] T. Y. Abay and P. A. Kyriacou, "Reflectance Photoplethysmography as Noninvasive Monitoring of Tissue Blood Perfusion," *IEEE Transactions on Biomedical Engineering,* vol. 62, no. 9, pp. 2187-2195, 2015.

[26] T. Miyata, T. Iwata and T. Araki, "A Reflection-Type Pulse Oximeter Using Four Wavelengths Equipped with a Gain-Enhanced Gated-Avalanche-Photodiode," in *13th International Conference on Biomedical Engineering - ICBME*, Singapore, 2008.

[27] D. Ahn and S. Hong, "Wireless Power Transmission With Self-Regulated Output Voltage for Biomedical Implant," *IEEE Transactions on Industrial Electronics,* vol. 61, no. 5, pp. 2225-2235, 2014.

[28] M. Makikawa, N. Shiozawa and S. Okada, "Chapter 7.1 - Fundamentals of Wearable Sensors for the Monitoring of Physical and Physiological Changes in Daily Life," in *Wearable Sensors*, Oxford, Academic Press, 2014, pp. 517-541.

[29] R. Yousefi, M. Nourani, S. Ostadabbas and I. Panahi, "A Motion-Tolerant Adaptive Algorithm for Wearable Photoplethysmographic Biosensors," *IEEE Journal of Biomedical and Health Informatics,* vol. 18, no. 2, pp. 670-681, 2014.

[30] E. A. Pelaez and E. R. Villegas, "LED power reduction trade-offs for ambulatory pulse oximetry," in *2007 29th Annual International Conference of the IEEE Engineering in Medicine and Biology Society*, Lyon, 2007.

[31] Y. T. Lin, Y. S. Lin, C. H. Chen, H. C. Chen, Y. C. Yang and S. S. Lu, "A 0.5-V Biomedical System-on-a-Chip for Intrabody Communication System," *IEEE Transactions on Industrial Electronics,* vol. 58, no. 2, pp. 690-699, 2011.

[32] O. Guven, F. Geier, D. Banks and C. Toumazou, "An open-source platform for the development of microcontroller based multi-wavelength oximetry," in *2010 Biomedical Circuits and Systems Conference (BioCAS)*, Paphos, 2010.

[33] P. Vaz, T. Pereira, E. Figueiras, C. Correia, A. Humeau-Heurtier and J. Cardoso, "Which wavelength is the best for arterial pulse waveform extraction using laser speckle imaging?," *Biomedical Signal Processing and Control,* vol. 25, pp. 188-195, 2016.

[34] B. Venema, J. Schiefer, V. Blazek, N. Blanik and S. Leonhardt, "Evaluating Innovative In-Ear Pulse Oximetry for Unobtrusive Cardiovascular and Pulmonary Monitoring During Sleep," *IEEE Journal of Translational Engineering in Health and Medicine,* vol. 1, pp. 2700208-2700208, 2013.

[35] L. S. Lovinsky, "Urgent problems of metrological assurance of optical pulse oximetry," *IEEE Transactions on Instrumentation and Measurement,* vol. 55, no. 3, pp. 869-875, 2006.

[36] Y. Pole, "Evolution of the pulse oximeter," *International Congress Series,* vol. 1242, pp. 137-144, 2002.

[37] Maxim Integrated Products, Inc, "MAX30100 - Pulse Oximeter and Heart-Rate Sensor IC for Wearable Health," 2014.

[38] R. G. Lyons, Understanding Digital Signal Processing, Michigan: Prentice Hall, 2010.

[39] S. Golestan, M. Ramezani, J. M. Guerrero, F. D. Freijedo and M. Monfared, "Moving Average Filter Based Phase-Locked Loops: Performance Analysis and Design Guidelines," *IEEE Transactions on Power Electronics,* vol. 29, no. 6, pp. 2750-2763, 2014.

[40] D. Cruz, E. Rodrigues, R. Godina, C. Cabrita, J. Matias and J. Catalão, "Novel methodology for integrated analog front-end signal processing blocks based portable multifunctional sensor for biomedical applications," in *IEEE International Conference on Environment and Electrical Engineering*, Florence, Italy, 2016.

[41] Q. Peng, C. Zhang, X. Zhao, X. Sun, F. Li, H. Chen and Z. Wang, "A Low-Cost UHF RFID System With OCA Tag for Short-Range Communication," *IEEE Transactions on Industrial Electronics,* vol. 62, no. 7, pp. 4455-4465, 2015.

[42] B. Venema, N. Blanik, V. Blazek, H. Gehring, A. Opp and S. Leonhardt, "Advances in Reflective Oxygen Saturation Monitoring With a Novel In-Ear Sensor System: Results of a Human Hypoxia Study," *IEEE Transactions on Biomedical Engineering,* vol. 59, no. 7, pp. 2003-2010, 2012.

[43] P. B. Batchelder and D. M. Raley, “Maximizing the laboratory setting for testing devices and understanding statistical output in pulse oximetry,” *Anesthesia & Analgesia,* vol. 105, no. 6, pp. S85-S94, 2007.

[44] R. Krishnan, B. Natarajan and S. Warren, “Two-Stage Approach for Detection and Reduction of Motion Artifacts in Photoplethysmographic Data,” *IEEE Transactions on Biomedical Engineering,* vol. 57, no. 8, pp. 1867-1876, 2010.

[45] R. Wijshoff, M. Mischi and R. Aarts, “Reduction of periodic motion artifacts in photoplethysmography,” *IEEE Transactions on Biomedical Engineering,* vol. in press, 2016.

[46] A. M. Tăuţan, A. Young, E. Wentink and F. Wieringa, “Characterization and reduction of motion artifacts in photoplethysmographic signals from a wrist-worn device,” in *2015 37th Annual International Conference of the IEEE Engineering in Medicine and Biology Society (EMBC)*, Milan, 2015.